# Conformational Dynamics of hSGLT1 during $Na^+$/Glucose Cotransport

Donald D.F. Loo, Bruce A. Hirayama, Movses H. Karakossian, Anne-Kristine Meinild, and Ernest M. Wright

Department of Physiology, David Geffen School of Medicine at UCLA, University of California, Los Angeles, CA 90095

This study examines the conformations of the $Na^+$/glucose cotransporter (SGLT1) during sugar transport using charge and fluorescence measurements on the human SGLT1 mutant G507C expressed in *Xenopus* oocytes. The mutant exhibited similar steady-state and presteady-state kinetics as wild-type SGLT1, and labeling of Cys507 by tetramethylrhodamine-6-maleimide had no effect on kinetics. Our strategy was to record changes in charge and fluorescence in response to rapid jumps in membrane potential in the presence and absence of sugar or the competitive inhibitor phlorizin. In $Na^+$ buffer, step jumps in membrane voltage elicited presteady-state currents (charge movements) that decay to the steady state with time constants $\tau_{med}$ (3–20 ms, medium) and $\tau_{slow}$ (15–70 ms, slow). Concurrently, SGLT1 rhodamine fluorescence intensity increased with depolarizing and decreased with hyperpolarizing voltages ($\Delta F$). The charge vs. voltage (Q-V) and fluorescence vs. voltage ($\Delta F$-V) relations (for medium and slow components) obeyed Boltzmann relations with similar parameters: $z\delta$ (apparent valence of voltage sensor) $\approx 1$; and $V_{0.5}$ (midpoint voltage) between $-15$ and $-40$ mV. Sugar induced an inward current ($Na^+$/glucose cotransport), and reduced maximal charge ($Q_{max}$) and fluorescence ($\Delta F_{max}$) with half-maximal concentrations ($K_{0.5}$) of 1 mM. Increasing $[\alpha MDG]_o$ also shifted the $V_{0.5}$ for Q and $\Delta F$ to more positive values, with $K_{0.5}$'s $\approx 1$ mM. The major difference between Q and $\Delta F$ was that at saturating $[\alpha MDG]_o$, the presteady-state current (and $Q_{max}$) was totally abolished, whereas $\Delta F_{max}$ was only reduced 50%. Phlorizin reduced both $Q_{max}$ and $\Delta F_{max}$ ($K_i \approx 0.4$ μM), with no changes in $V_{0.5}$'s or relaxation time constants. Simulations using an eight-state kinetic model indicate that external sugar increases the occupancy probability of inward-facing conformations at the expense of outward-facing conformations. The simulations predict, and we have observed experimentally, that presteady-state currents are blocked by saturating sugar, but not the changes in fluorescence. Thus we have isolated an electroneutral conformational change that has not been previously described. This rate-limiting step at maximal inward $Na^+$/sugar cotransport (saturating voltage and external $Na^+$ and sugar concentrations) is the slow release of $Na^+$ from the internal surface of SGLT1. The high affinity blocker phlorizin locks the cotransporter in an inactive conformation.

The Journal of General Physiology

## INTRODUCTION

The $Na^+$/glucose cotransporter, SGLT1, is a member of a large family of proteins (SLC5) that uses the $Na^+$ electrochemical gradient to transport substrates (sugars, amino acids, osmolytes, neurotransmitters, ions, and water) against their concentration gradients. We have proposed that the protein functions by an alternating access mechanism, and a simplified six-state ordered kinetic model has been proposed (Parent et al., 1992b; Loo et al., 1998). In previous studies, we characterized the voltage-dependent partial reactions of SGLT1 in the absence of glucose using charge and fluorescence measurements on an hSGLT1 mutant Q457C where sugar transport is abolished after labeling of Cys457 by the fluorophore tetramethylrhodamine-6-maleimide (TMR6M) (Loo et al., 1998, 2005; Meinild et al., 2002). Our conclusion was that the presteady-state currents (in the absence of glucose) are associated with $Na^+$ binding, and isomerization of the empty carrier involves a series of four conformational changes (Loo et al., 2005).

The goal of the present study is to examine the conformations of the transporter under sugar transport conditions. Our kinetic model predicts that the conformational occupancy distribution of the transporter depends on the sugar concentration. We expressed hSGLT1 mutant G507C in *Xenopus laevis* oocytes and recorded changes in transporter currents (steady state and presteady state) and rhodamine fluorescence after step jumps in membrane voltage. The mutant transporter has similar steady-state and presteady-state kinetics as hSGLT1, before and after labeling of Cys507 by TMR6M. The charge and fluorescence measurements provide independent and complementary views of protein conformational changes. Our model predicts that the charge movements in the $Na^+$/glucose cotransport

Correspondence to Donald Loo: dloo@mednet.ucla.edu

M.H. Karakossian's present address is Department of Neurobiology, David Geffen School of Medicine at UCLA.

A.-K. Meinild's present address is August Krogh Institute, University of Copenhagen, Universitetsparken 13, Copenhagen 2100, Denmark.

Abbreviations used in this paper: au, arbitrary unit of fluorescence intensity; SGLT1, $Na^+$/glucose cotransporter; hSGLT1, human $Na^+$/glucose cotransporter; αMDG, α-methyl-D-glucopyranoside; TMR6M, tetramethylrhodamine-6-maleimide; MTSEA, 2-aminoethyl methanethiosulfonate hydrobromide.

cycle are associated with external $Na^+$ binding and translocation of the empty transporter, whereas changes in fluorescence could originate from any (or all) of the conformational transitions of the transport cycle. By using a fully functional protein, we are now able to study the partial reactions involved in sugar binding and translocation. We expected that the fluorescence measurements would reveal conformations not detected by charge measurements. Our data do uncover a novel, slow conformational change with sugar transport that is not associated with charge movement, and simulations indicate that this is due to a slow electroneutral step in the transport cycle associated with the release of $Na^+$ from SGLT1 in the internal membrane surface. We found that sugar shifted the conformations of SGLT1, resulting in a reduction in the occupancy probability in the outward-facing, and increasing the occupancy probability in the inward-facing, $Na^+$-bound conformations. Phlorizin, the high affinity inhibitor, locked the transporter in the phlorizin-bound form and proportionally reduced the occupancy probabilities in all other conformations.

## MATERIALS AND METHODS

### Preparation and Maintenance of Oocytes

Mature *Xenopus laevis* oocytes were isolated, defolliculated, and injected with hSGLT1 or hSGLT1 mutant G507C cRNA (see Loo et al., 1993, 1998). The G507C mutant was constructed using standard PCR techniques and confirmed by DNA sequencing. Oocytes expressing hSGLT1 G507C were labeled with TMR6M (Invitrogen; Loo et al., 1998; Meinild et al., 2002). We determined the maximal fluorescence change ($\Delta F_{max}$, see below) as a function of the incubating $[TMR6M]_o$ (from 1 to 100 μM) and duration of labeling (from 1 to 30 min), and found that the extent of labeling of Cys 507C by the fluorophore was saturating in 100 μM $[TMR6M]_o$ for 10 min in NaCl buffer at the normal resting membrane potential. We assume that all the functional transporters are labeled. After labeling, oocytes were washed free of dye and kept in NaCl buffer in the dark until use. MTSEA (2-aminoethyl methanethiosulfonate hydrobromide; Toronto Research Biochemicals) was prepared and used as previously described (Loo et al., 1998). Oocytes were bathed in a NaCl buffer containing (in mM) 100 NaCl, 2 KCl, 1 $CaCl_2$, 1 $MgCl_2$, 10 HEPES, pH 7.4. αMDG or phlorizin was added to the superfusing NaCl buffer at the reported concentrations. $Na^+$ concentration was varied by equimolar replacement of $Na^+$ with choline.

### Uptake Experiments

Sugar uptake into oocytes was measured using 50 μM $^{14}$C-α-methyl-D-glucopyranoside ($^{14}$C-αMDG, Amersham Biosciences), a nonmetabolized sugar analogue that is transported by human SGLT1 (see Ikeda et al., 1989). The initial rates of sugar uptake into oocytes were measured at 20–23°C for 10–60 min. Experiments were repeated at least twice on oocytes isolated from different donor frogs. Uptake was expressed in pmol per oocyte per minute (mean ± SEM).

### Combined Electrophysiological and Fluorescence Experiments

Electrophysiological and fluorescence experiments were performed simultaneously, using two-electrode voltage clamp fluorometry (Loo et al., 1998, 2005; Meinild et al., 2002). A standard pulse protocol was applied where membrane potential was held at −50 mV ($V_h$) and stepped to various test potentials ($V_t$ from +90 to −150 mV in 20 mV decrements) for 100 (or 500) ms before returning to $V_h$. The current records were the averages of three sweeps, and the fluorescence records were averages of either 3 or 10 sweeps. To minimize the effects of photobleaching, the 500-ms fluorescence records were averages of three sweeps. Records were filtered at 500 or 50 Hz, depending on the sampling interval (0.1 or 0.5 ms per sample). Note that in the present studies, we do not record the fast components of ΔF observed in our previous study using cut-open oocyte voltage clamp fluorometry (Loo et al., 2005). Fluorescence intensity is expressed as arbitary units (au). In TMR6M-labeled oocytes expressing mutant G507C bathed in NaCl buffer, $\Delta F_{max}/F_{total}$ is ≈1%, where $\Delta F_{max}$ is the maximal fluorescence intensity change and $F_{total}$ is the total fluorescence intensity. Fluorescence data have been corrected for photobleaching and rundown (Meinild et al., 2002). All experiments were performed at room temperature (20–23°C).

### Data Analysis

*Steady-State Currents.* To obtain the current–voltage (I-V) relations of the sugar-induced current, the pulse protocol was applied with 100-ms pulses. The sugar-induced current was obtained by subtracting the current in NaCl buffer (measured at 100 ms) from the current with sugar (αMDG) added to the external solution. The substrate-induced currents (at each voltage) were fitted to the equation

$$I = I_{max}([S]_o)^n/\{(K_{0.5})^n + ([S]_o)^n\}, \quad (1)$$

where $I_{max}$ is the maximal current, $[S]_o$ is the external substrate (αMDG or $Na^+$) concentration, $K_{0.5}$ is the half-maximal substrate concentration ($[S]_o$ at 50% $I_{max}$), and n is the Hill coefficient. For the kinetics of sugar activation, n was fixed at 1 (Birnir et al., 1991; Parent et al., 1992a; Mackenzie et al., 1998).

*Isolation of Presteady-State Currents.* Total membrane current in response to a voltage pulse consisted of the bilayer capacitive transient, the presteady-state currents of SGLT1, and the steady-state currents. In the absence of external sugar, the steady-state currents consisted of the background (endogenous) currents of the oocyte and the $Na^+$ leak (uniporter mode) mediated by SGLT1 (Parent et al., 1992b; Loo et al., 1998). We found previously that the presteady-state currents of hSGLT1 (in the absence of external sugar) contained three components, with time constants ($\tau$) ranging from fast (0.2–1.5 ms), medium (3–20 ms), and slow (30–160 ms), and the method of isolating the three components has been described in detail (Loo et al., 2005). The focus of this study is the medium component, as the fast component is beyond the resolution of the two-electrode voltage clamp (≈1 ms). Since the kinetics of the medium component ($\tau$-V and Q-V relations) obtained from records corrected for the slow component (describe above) are similar to those obtained from uncorrected records (Loo et al., 2005), the medium component was estimated from uncorrected records using 100-ms voltage pulses (Loo et al., 1993; Hazama et al., 1997; Quick et al., 2001; Meinild et al., 2002). In these experiments, total current relaxation ($I_{tot}$) was fitted to the equation

$$I_{tot}(t) = I_{cm}\exp(-t/\tau_{cm}) + I_{med}\exp(-t/\tau_{med}) + I_{ss}, \quad (2)$$

where $I_{ss}$ is the steady-state current, $I_{cm}\exp(-t/\tau_{cm})$ is the bilayer capacitance current with initial value $I_{cm}$ and time constant $\tau_{cm}$, and $I_{med}\exp(-t/\tau_{med})$ is the medium component of SGLT1 presteady-state current with initial value $I_{med}$ and time constant $\tau_{med}$. The medium component of presteady-state current ($I_{med}\exp(-t/\tau_{med})$

was isolated by subtraction of the steady-state ($I_{ss}$) and membrane bilayer capacitance ($I_{cm}\exp(-t/\tau_{cm})$) from the total current. The medium charge movement associated with SGLT1 was obtained from the integral of the medium component of presteady-state current. This analysis was extended to the presteady-state current (or carrier transients) in the presence of sugar. At steady state, the current ($I_{ss}$) consisted of the oocyte background current, $Na^+$-uniporter current (of SGLT1), and the $Na^+$/sugar cotransport current.

In experiments where the slow and medium components were isolated (Fig. 2), 100- and 500-ms pulses were applied (Fig. 2, A and B). The slow time constant ($\tau_{slow}$) was estimated from the 500-ms current records after the medium component has decayed (the period was five times the time constant of the medium component, see Fig. 2 of Loo et al., 2005 for detailed description). The early phase was obtained by extrapolation of the exponential fit to the peak of the capacitive transient, typically two sample points after onset of the voltage pulse. The slow charge was obtained from the integral of the slow component of presteady-state current. The medium charge was then estimated using 100-ms pulses after subtraction for the slow component and steady-state current.

*Fitting of Q-V and ΔF-V Relations.* The charge vs. voltage ($Q\text{-}V_m$) relations for medium and slow charge could, to a first approximation, be fitted to a single Boltzmann function (Loo et al., 1993; Hazama et al., 1997):

$$(Q - Q_{hyp})/Q_{max} = 1/[1 + \exp(z\delta(V_m - V_{0.5})F/RT], \quad (3)$$

where $Q_{max} = Q_{dep} - Q_{hyp}$, $Q_{dep}$ and $Q_{hyp}$ are the Q (absolute value) at depolarizing and hyperpolarizing limits, $V_m$ is membrane potential, F is the Faraday, R is the gas constant, T is the absolute temperature, $V_{0.5}$ is the membrane potential at 50% $Q_{max}$ (or the midpoint voltage), and $z\delta$ is the maximum steepness factor for the dependence of Q on voltage, or the apparent valence of the voltage sensor. $z\delta$ is the product of the apparent valence of the movable charge (z), and the fraction of the membrane electric field traversed by the charge ($\delta$). We denote $z\delta_Q$ for $z\delta$ obtained from charge movement.

The Boltzmann relation was also used to empirically fit the dependence of the change of fluorescence intensity ($\Delta F$) on membrane voltage (Loo et al., 1998; Meinild et al., 2002). The parameters obtained were the maximal fluorescence intensity change ($\Delta F_{max}$), the membrane voltage at 50% $\Delta F_{max}$ ($V_{0.5}^F$), and the apparent valence or voltage-steepness factor for fluorescence ($z\delta_F$).

Fits of data to equations were performed using either Sigmaplot 2002 (SPSS), or Clampfit 8.1 (Axon Instruments, Inc.). On data obtained on a single oocyte, the statistics are given by the estimates and the standard error of the fit. When data is from a population, the statistics are given by the means and standard errors of the means with the number of samples. While data are shown for representative experiments, all experiments were performed on at least three oocytes from different batches.

## Simulation of SGLT1

The differential equation for the eight-state model for $Na^+$/glucose cotransport (Fig. 9) is shown as Eq. 4 (below). $C_i$ is the occupancy probability in state i, and $C_1 + C_2 + C_3 + C_4 + C_5 + C_6 + C_a + C_b = 1$. Excluding the substrate-binding reactions, the rate constants $k_{ij}$ for transitions from $C_i \rightarrow C_j$ are given by $k_{ij} = k_{ij}^o \exp(-\varepsilon_{ij}F/RT)$, where $k_{ij}^o$ is a voltage-independent rate, $\varepsilon_{ij}$ is the equivalent charge movement (up to the transition state from $C_i \rightarrow C_j$), and F, R, and T have their usual physicochemical meanings (Parent et al., 1992b). $Na^+$ and sugar binding to the protein on the external and internal membrane surfaces is represented by pseudo-rate constants $k_{12} = k_{12}^o [Na]_o^2 \exp(-\varepsilon_{12}FV/RT)$, $k_{23} = k_{23}^o[\alpha MDG]_o$, $k_{65} = k_{65}^o[Na]_i^2$, and $k_{54} = k_{54}^o[\alpha MDG]_i$. There are four components of presteady-state current associated with voltage-sensitive reactions (shaded region of Fig. 9): $C_2 \rightleftarrows C_1$, $C_1 \rightleftarrows C_a$, $C_a \rightleftarrows C_b$, and $C_b \rightleftarrows C_6$. The presteady-state current ($I_{ij}$) due to $C_i \rightleftarrows C_j$ was calculated by $I_{ij} = e(\varepsilon_{ij} + \varepsilon_{ji})(k_{ij}C_{ij} - k_{ji}C_j)$, where e is the elementary charge (Parent et al., 1992b; Loo et al., 2005). The total SGLT1 current (I) is $I = N_T (I_{12} + I_{1a} + I_{ab} + I_{b6})$, where $N_T$ is the total number of transporters in the oocyte plasma membrane. The simulations shown in Figs. 10–13 and Table I were performed for wild-type hSGLT1 and TMR6M-labeled mutant G507C at 20°C using the parameters of Table II with $[Na^+]_o$ = 100 mM, $[Na^+]_i$ = 5 mM, $[\alpha MDG]_i = 0$, and $N_T = 10^{10}$ transporters. All the simulations were performed at 0–100 mM $[Na^+]_o$ and 0–100 mM $[sugar]_o$.

External phlorizin was assumed to bind to SGLT1 in the $Na^+$-bound conformation (Parent et al., 1992b): $[CNa_2]' \rightleftarrows [CNa_2Pz]'$, thus in the presence of phlorizin, there are nine states (Fig. 9). Simulations of the phlorizin-binding model (using the rate constants of Table II) were performed in a similar manner to the eight-state model, with modifications to include the phlorizin-bound state $[CNa_2Pz]'(C_7)$: $C_1 + C_2 + C_3 + C_4 + C_5 + C_6 + C_a + C_b + C_7 = 1$; $d/dt\ C_7 = -k_{72}C_7 + k_{27}C_2$ ; and $d/dt\ C_2 = -(k_{21} + k_{25} + k_{23} + k_{27})C_2 + k_{12}C_1 + k_{52}C_5 + k_{32}C_3 + k_{72}C_7$.

Computer simulations were performed using Berkeley Madonna 8.0.1. The voltage pulse protocol was simulated by determining the initial occupancy probabilities at the holding potential ($V_h = -50$ mV), and as membrane potential was stepped to each test value ($V_t$ ranging between +50 and −150 mV), the time course of the occupancy probabilities, cotransporter currents, and fluorescence ($\Delta F$) were obtained by numerically integrating the differential equation (Eq. 4) using the Runge-Kutta Method. Steady-state kinetic parameters were simulated by generating the I-V relations as functions of $[Na^+]_o$ and $[sugar]_o$. Kinetic parameters $I_{max}$, $K_{0.5}$, and n (at each $V_m$) were obtained by fitting the I vs. $[sugar]_o$ (or $[Na^+]_o$) relations to Eq. 1.

For presteady-state simulations, the transient cotransporter currents for the ON and OFF responses at each test voltage ($V_t$) were integrated to obtain the charge (Q). The Q vs. $V_t$ relations were fitted with the Boltzmann relation (Eq. 3) to obtain the maximal charge ($Q_{max}$), apparent valence of the voltage sensor ($z\delta_Q$), and midpoint voltage ($V_{0.5}$). The eigenvalues of the matrix (Eq. 4) were obtained using MATLAB 6.0 (The MathWorks Inc.). The time constants were the reciprocals of the eigenvalues (Loo et al., 2005).

$$d/dt \begin{bmatrix} C_1 \\ C_2 \\ C_3 \\ C_4 \\ C_5 \\ C_6 \\ C_a \\ C_b \end{bmatrix} = \begin{bmatrix} -(k_{1a}+k_{12}) & k_{21} & 0 & 0 & 0 & 0 & k_{a1} & 0 \\ k_{12} & -(k_{21}+k_{23}+k_{25}) & k_{32} & 0 & k_{52} & 0 & 0 & 0 \\ 0 & k_{23} & -(k_{32}+k_{34}) & k_{43} & 0 & 0 & 0 & 0 \\ 0 & 0 & k_{34} & -(k_{43}+k_{45}) & k_{54} & 0 & 0 & 0 \\ 0 & k_{25} & 0 & k_{45} & -(k_{54}+k_{56}+k_{52}) & k_{65} & 0 & 0 \\ 0 & 0 & 0 & 0 & k_{56} & -(k_{65}+k_{6b}) & 0 & k_{b6} \\ k_{1a} & 0 & 0 & 0 & 0 & 0 & -(k_{a1}+k_{ab}) & k_{ba} \\ 0 & 0 & 0 & 0 & 0 & k_{6b} & k_{ab} & -(k_{ba}+k_{b6}) \end{bmatrix} \begin{bmatrix} C_1 \\ C_2 \\ C_3 \\ C_4 \\ C_5 \\ C_6 \\ C_a \\ C_b \end{bmatrix} \quad (4)$$

Fluorescence experiments were simulated by assuming that changes of fluorescence intensity ($\Delta F$) with step jumps in membrane voltage are due to changes in occupancy probabilities: $\Delta F \approx q_{y_1}\Delta C_1 + q_{y_2}\Delta C_2 + q_{y_a}\Delta C_a + q_{y_b}\Delta C_b + q_{y_3}\Delta C_3 + q_{y_4}\Delta C_4 + q_{y_5}\Delta C_5 + q_{y_6}\Delta C_6$, where $q_{y_j}$ is the apparent quantum yield of the fluorophore (TMR6M) when SGLT1 is in conformation $C_j$. The simulations were performed with $q_{y_1} = 3$, $q_{y_2} = 1$, $q_{y_a} = 3$, $q_{y_b} = 3$, $q_{y_4} = 3$, $q_{y_5} = 3$, and $q_{y_6} \approx 5$–6. In practice, $\Delta F$ was determined by the relative quantum yields $q_{y_5}/q_{y_2} \approx 3$, and $q_{y_6}/q_{y_2} \approx 6$ (see Discussion below).

The Dixon analysis (for the determination of the inhibitory constant $K_i$ for phlorizin, Table I) was simulated by determining the intersection of the straight lines $-1/I$ vs. $[\text{phlorizin}]_o$ relations at $[\alpha\text{MDG}]_o = 1$ and 2 mM, where I is the sugar-coupled current (at −150 mV) at each $[\text{phlorizin}]_o$ (see Panayotova-Heiermann et al., 1995). $[\text{Phlorizin}]_o$ used was 0, 50, 100, 200, 500, 1,000, 5,000, and 10,000 nM.

## RESULTS

### Part I. Steady- and Presteady-State Kinetics

We first briefly describe the steady-state kinetic properties of hSGLT1 G507C, and the effects of MTSEA and TMR6M. The kinetics of the presteady-state currents in the absence of glucose and the fluorescence changes of the TMR6M-labeled mutant protein with step jumps in membrane voltage are then presented. These provide the basis for describing the conformations of SGLT1 under sugar-transporting conditions by charge and fluorescence measurements (Part II).

### Steady-State Kinetics

*$^{14}$C-αMDG Uptake.* The rates of $^{14}$C-αMDG (50 μM) uptake into oocytes were comparable for oocytes expressing the mutant transporter and wild-type hSGLT1. In a representative experiment on the same batch of oocytes (each determination being the mean of 8–10 oocytes and expressed as the mean ± SEM), in the presence of external $Na^+$ (100 mM), uptake by oocytes injected with hSGLT1 G507C-cRNA was 143 ± 8 pmol/oocyte/h versus 176 ± 10 pmol/oocyte/h for oocytes injected with wild-type hSGLT1-cRNA. This uptake rate was 100-fold greater than that of noninjected oocytes (1.4 ± 0.1 pmol/oocyte/h). Uptake of αMDG by hSGLT1 G507C was dependent on external $Na^+$ and blocked by the SGLT1-specific inhibitor phlorizin. When external $Na^+$ was replaced by choline, the rate of sugar uptake (1.6 ± 0.1 pmol/oocyte/h) was similar to that of noninjected control oocytes (0.6 ± 0.1 pmol/oocyte/h). Phlorizin (500 μM) in the external solution also reduced the rate of $^{14}$C-αMDG uptake by the mutant to that of controls.

*$Na^+$ and Sugar Activation.* The total current from an oocyte expressing hSGLT1 G507C in NaCl buffer is shown in Fig. 1 A. Membrane potential ($V_m$) was held at −50 mV ($V_h$) and stepped to a series of test values for 100 ms (from +50 to −150 mV) before returning to $V_h$. The current relaxation consisted of an initial membrane capacitive transient (time constant $\tau \approx 0.8$ ms) followed by the decay of the presteady-state current to steady state (with $\tau \approx$ 3–20 ms) (Loo et al., 1993, 2005). The current records when 1 mM αMDG was added to the bathing medium are shown in Fig. 1 B. At each test voltage, αMDG increased the steady-state current, and there was a shift in the profile of the presteady-state current records. This is particularly noticeable in the OFF response when the test voltage was returned to $V_h$ (the effect of sugar on presteady-state current will be presented below).

The current vs. voltage (I-V) relation of the αMDG-induced current tended toward saturation at large negative membrane voltages (−150 mV) and approached zero at +50 mV (Fig. 1 C). At each voltage, the I vs. $[\alpha\text{MDG}]_o$ relation was hyperbolic (e.g., Fig. 1 D shows the relation at −50 mV). The half-maximal concentration for αMDG ($K_{0.5}^{\alpha MDG}$) was 1.6 mM. $K_{0.5}^{\alpha MDG}$ decreased with negative membrane voltages (Fig. 1 E), and reached a minimum of 1.0 ± 0.1 mM at −150 mV. In three experiments, at 100 mM $[Na^+]_o$ and −50 mV, $K_{0.5}^{\alpha MDG}$ was 1.7 ± 0.3 mM.

The dependence of the αMDG-induced current on $[Na^+]_o$ was sigmoid. The Hill coefficient was 1.5 and independent of membrane voltage (unpublished data). Fig. 1 F shows the dependence of the half-maximal concentration for $Na^+$ ($K_{0.5}^{Na}$) on voltage. At −50 mV, $K_{0.5}^{Na}$ was 20 ± 2 mM and decreased to 2.8 ± 0.4 mM at −150 mV. In three experiments, $K_{0.5}^{Na}$ at −50 mV was 18 ± 1 mM.

*Effects of MTSEA and TMR6M.* The rate of $^{14}$C-αMDG uptake for oocytes expressing hSGLT1 mutant G507C preincubated in MTSEA (1 mM for 15 min in NaCl buffer) was 81 ± 14% ($n = 5$) of the control nontreated oocytes, indicating that the mutant hSGLT1 G507C retained the ability to transport sugar after Cys507 was modified by MTSEA. We confirmed that the Cys507 was derivatized by MTSEA from the reduction in maximal fluorescence change ($\Delta F_{max}$, see Fig. 3 below) after the oocytes were preincubated in the reagent. In four experiments, compared with control nonpreincubated oocytes, $\Delta F_{max}$ (measured with the oocytes bathed in NaCl buffer) was reduced 93% (from 9.1 ± 1.0 au to 0.06 ± 0.14 au). In control experiments on oocytes expressing wild-type hSGLT1, exposure to MTSEA had no effect on the kinetics of hSGLT1 (see also Loo et al., 1998), and after labeling by TMR6M, fluorescence changes induced by voltage jumps were not observed in noninjected oocytes and hSGLT1-expressing oocytes (unpublished data).

The affinity for sugar was unaffected by either MTSEA or TMR6M. In representative experiments on the same oocytes (at −50 mV), $K_{0.5}^{\alpha MDG}$ was 1.9 ± 0.1 mM before, 2.0 ± 0.2 mM after MTSEA, and 2.4 ± 0.3 mM after TMR6M. The I-V curves of the sugar-induced currents

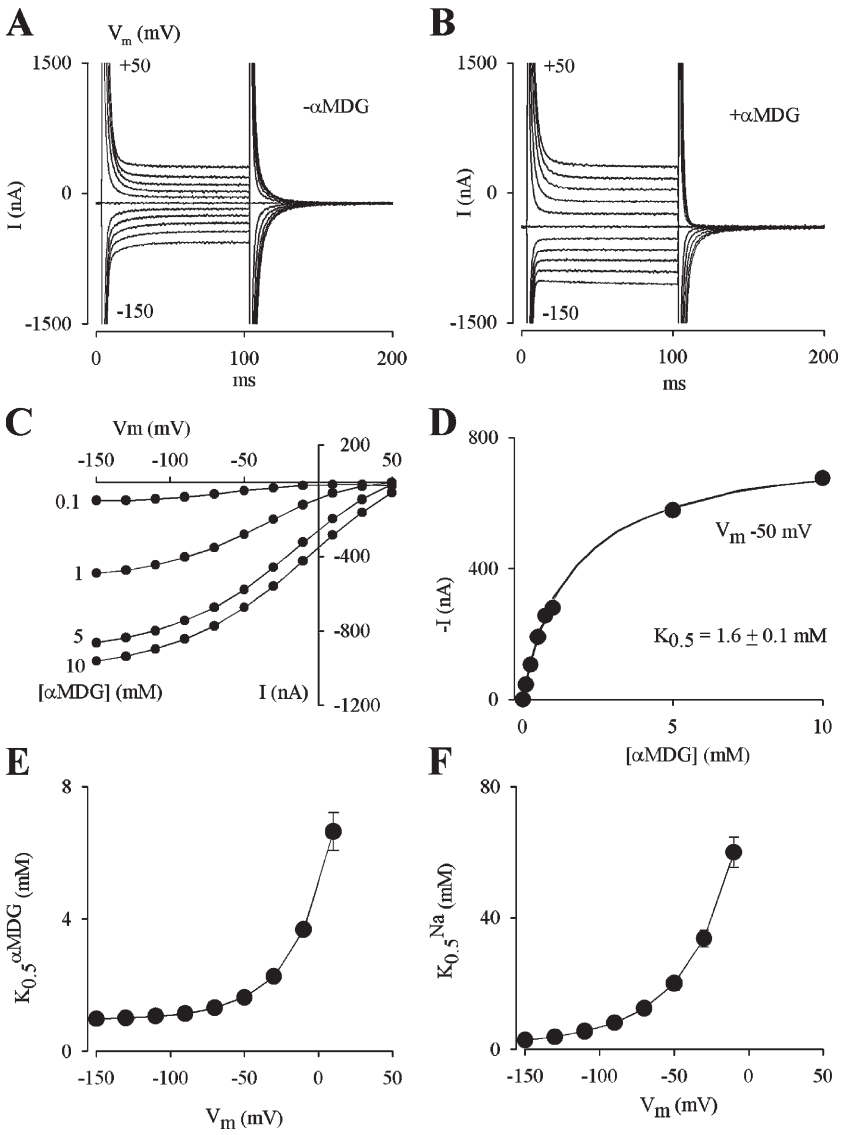


**Figure 1.** Steady-state kinetics of G507C. (A) Total current records from an hSGLT1 G507C cRNA-injected oocyte that had been labeled with TMR6M. Membrane potential ($V_m$) was held at −50 mV ($V_h$), and then stepped to a test value ($V_t$, starting at +50 mV and ending at −150 mV in 20-mV decrements) for 100 ms before returning to $V_h$. The bath solution was NaCl buffer. (B) Total current records when 1 mM αMDG was added to the bath solution. (C) Steady-state I-V relations. The αMDG-induced current (0.1–10 mM) was obtained by subtracting the current (measured at 100 ms) with sugar added from baseline current in $Na^+$ alone. (D) Dose–response relation for αMDG-induced current. $[Na^+]_o$ = 100 mM, and $V_m$ = −50 mV. The curve was the fit (Eq. 1) to the data: $I_{max}$ = 778 ± 13 nA, and $K_{0.5}^{αMDG}$ = 1.6 ± 0.1 mM. (E) Voltage dependence of $K_{0.5}^{αMDG}$. (F) Voltage dependence of $K_{0.5}^{Na}$. Experiment was performed by increasing $[Na^+]_o$ (from 0 to 100 mM) with $[αMDG]_o$ maintained at 25 mM. Errors bars are standard errors (SE) of the fit when SE exceeds the size of the symbol.

(at 20 mM αMDG) between MTSEA-labeled and nonlabeled oocytes were similar, except for a slight reduction (6 ± 4%, $n$ = 5) in the current at each voltage.

### Presteady-State Kinetics

*Charge Movement.* We have previously found that in two-electrode voltage clamp experiments on hSGLT1, the presteady-state currents contained medium and slow components with time constants of 3–20 and 30–100 ms (Loo et al., 2005). Similar time constants were also observed in mutant hSGLT1 G507C (Fig. 2). Like wild-type hSGLT1, the transient currents of the mutant did not quite reach steady state at 100 ms (Fig. 2 A), and there was a slow decay to steady state revealed in the 500-ms pulses (Fig. 2 B).

The τ-V relation for the medium component is shown in Fig. 2 C. For the ON pulse, when membrane potential was stepped from $V_h$ to $V_t$, $\tau_{med}$ was 20 ± 1 ms at −150 mV and decreased to 4.0 ± 0.2 ms at +50 mV (filled symbols). For the OFF pulse, when $V_t$ was returned to $V_h$, $\tau_{med}$ was independent of the test voltage (open symbol), and was 12 ± 1 ms ($n$ = 10). The medium charge transfer ($Q_{med}$), obtained by integrating the medium component of presteady-state current, was the same for the ON and OFF. The $Q_{med}$-V relation is shown in Fig. 2 D. The line was the fit of the data by a Boltzmann relation with a maximal charge ($Q_{max}$) of 12 nC, apparent valence ($z\delta_Q$) of 1.0, and midpoint voltage ($V_{0.5}$) of −44 mV.

The τ-V relation for slow charge was similar to the medium (Fig. 2 C). $\tau_{slow}$ for ON was maximal at hyperpolarizing voltages (τ = 70 ms at −150 mV) and decreased as the test voltage was made positive (τ = 15 ms at +50 mV). $\tau_{slow}$ for OFF was also independent of voltage and was 39 ± 5 ms ($n$ = 10). The $Q_{slow}$-V curve obeyed the Boltzmann relation with a $Q_{max}$ of 7 nC, $z\delta_Q$ of 1.0, and a $V_{0.5}$ of −62 mV (Fig. 2 E). When the medium and slow charges were added to obtain the total charge ($Q_{total}$),

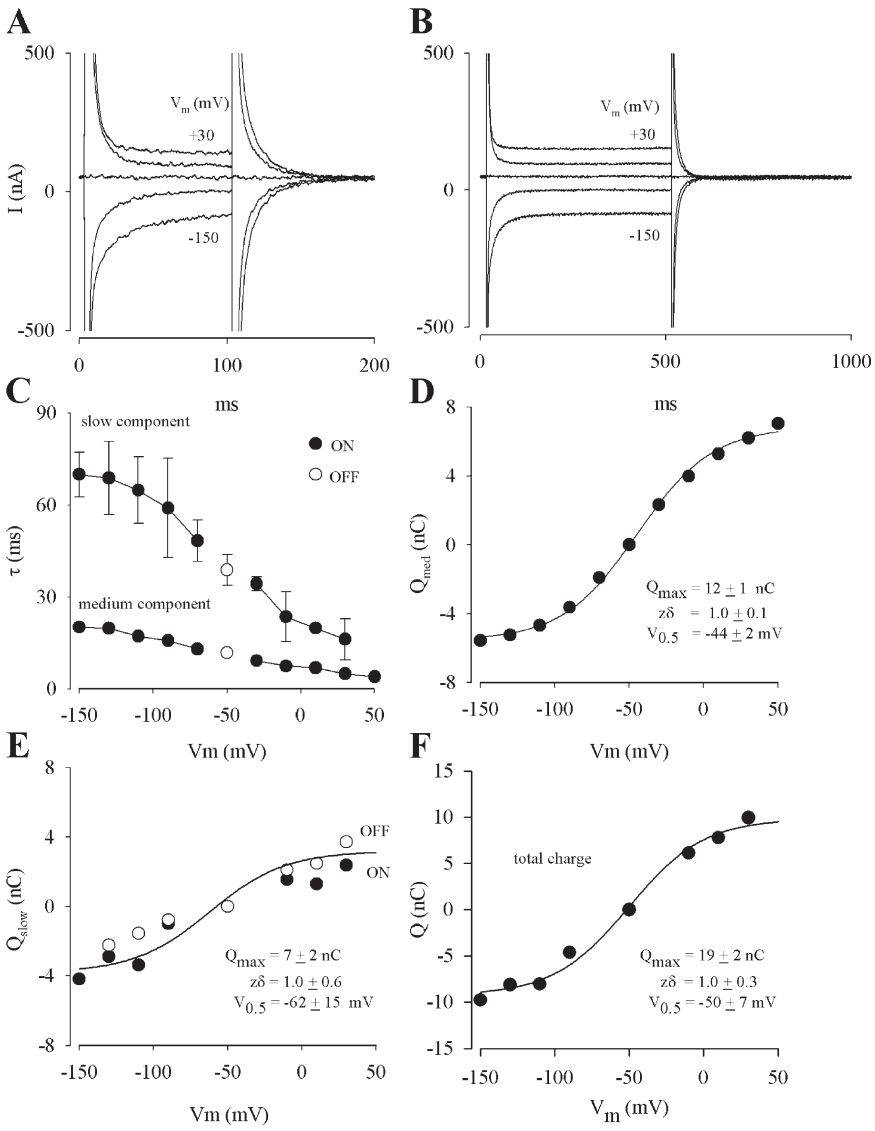


**Figure 2.** Presteady-state kinetics of hSGLT1 G507C (nonlabeled). (A) Current record for 100-ms test voltage pulses. $V_h$ was −50 mV, and the current records at selected $V_t$ = +30, −10, −50, −90, and −150 mV are shown for the ON and OFF pulses. (B) The corresponding current records for 500-ms pulses. (C) τ-V relation for the medium and slow components. The OFF responses were independent of the previous test potential ($V_t$), and the open symbol represents the mean of 10 values with $V_t$ varying between +50 and −150 mV. (D) Q-V relation for medium charge. (E) Q-V relation for slow charge. (F) Q-V relation for total charge. The curve in D was obtained from fitting the data with the Boltzmann relation (Eq. 3). In E and F, the Boltzmann fits were obtained under the constraint z = 1.0.

the $Q_{total}$-V curve followed the Boltzmann relation with a $Q_{max}$ of 19 nC, $z\delta_Q$ of 1.0, and $V_{0.5}$ of −50 mV (Fig. 2 F).

We focused our attention on the medium component and estimated medium charge from 100-ms pulses uncompensated for slow charge. Previously we found the $\tau_{med}$-V and $Q_{med}$-V relations obtained from current records corrected for slow charge were similar to those obtained from uncorrected records (Loo et al., 2005). For the medium component, the maximal charge ($Q_{max}$) ranged from 5 to 30 nC, depending on the level of expression of mutant G507C in the oocyte plasma membrane. $z\delta_Q$ was 1.0 ± 0.1 ($n$ = 6). $V_{0.5}$ ranged between −30 and −47 mV, with a mean of −38 ± 3 ($n$ = 6).

TMR6M did not affect the kinetics of the presteady-state currents. In a representative experiment on the same oocyte where we monitored the medium charge movement before and after TMR6M, $z\delta_Q$, $V_{0.5}$, and $Q_{max}$ were 0.9 ± 0.1, −30 ± 1 mV, and 18 ± 1 nC before, and 0.9 ± 0.1, −28 ± 1 mV, and 18 ± 1 nC after TMR6M. The population means for $z\delta_Q$ and $V_{0.5}$ after labeling by TMR6M were 1.0 ± 0.1 ($n$ = 6), and −35 ± 3 mV ($n$ = 6). $V_{0.5}$ ranged between −28 and −45 mV. The τ-V relations (for medium charge) were the same before and after labeling by TMR6M (unpublished data).

*Fluorescence.* The time course of the fluorescence signal (ΔF) from a TMR6M-labeled hSGLT1 G507C-expressing oocyte in response to a series of voltage pulses (from $V_h$ −50 mV) is shown in Fig. 3. Fluorescence intensity increased with depolarizing voltages and decreased with hyperpolarizing voltages. Fluorescence intensity returned to baseline when the test pulse was stepped back to $V_h$. Like charge movement, the fluorescence records consisted of medium and slow components. The slow component was much more apparent in the depolarizing direction, especially the OFF response (Fig. 3, A vs. B).

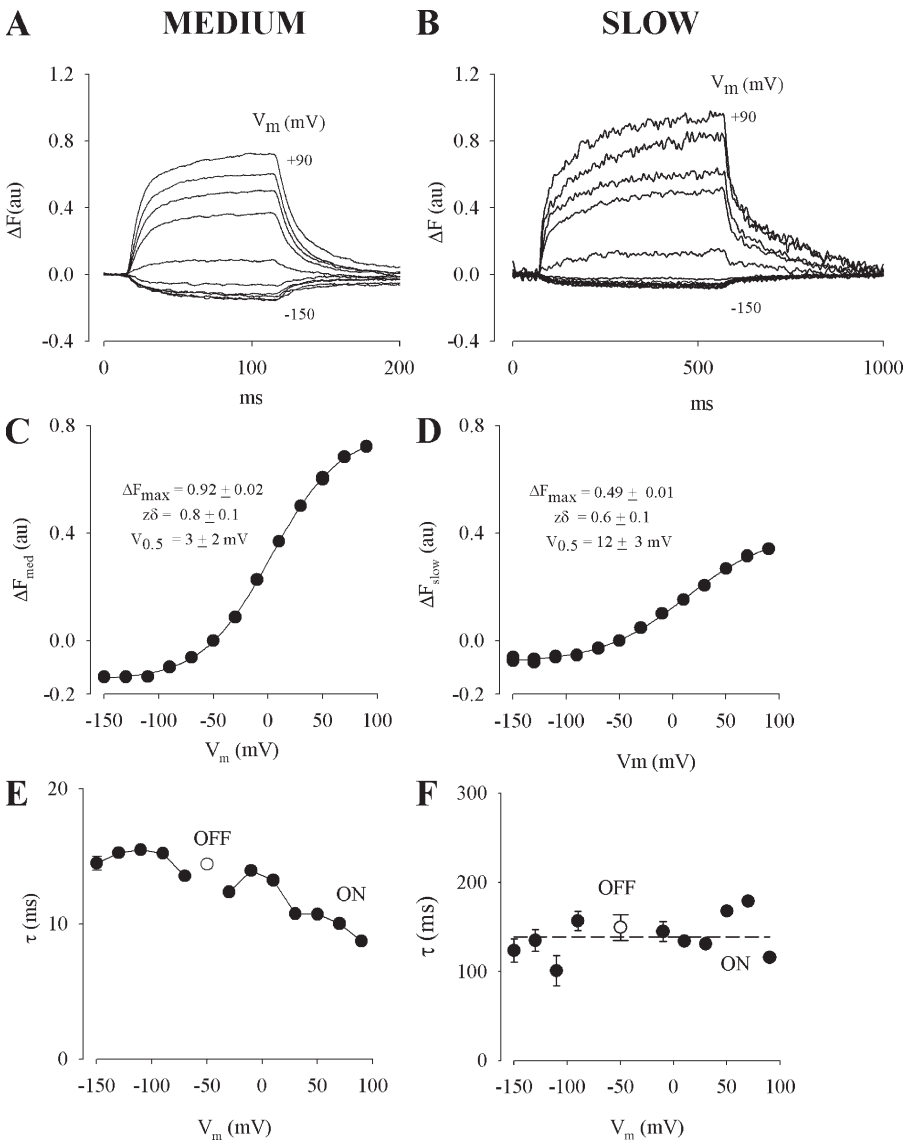


**Figure 3.** Changes of fluorescence intensity (ΔF) of TMR6M-labeled G507C hSGLT1 with step jumps in membrane voltage. Membrane was held at −50 mV and then stepped to various test voltages. (A) Time course of ΔF observed with selected 100-ms pulses. (B) Time course of ΔF observed with selected 500-ms pulses. To minimize photobleaching, the 500-ms records were averages of three records compared with 10 for 100-ms records, hence the greater apparent noise level of the former. (C) $\Delta F_{med}$-V relation. The line was the fit of the data with the Boltzmann relation. (D) $\Delta F_{slow}$-V relation. As in C, the line was the fit with the Boltzmann relation. (E) τ-V relation for the medium component of ΔF. (F) τ-V relation for the slow component of ΔF. The open symbols (in E and F) are the time constants τ for the OFF pulses.

The medium and slow components ($\Delta F_{med}$ and $\Delta F_{slow}$) at each voltage were isolated by fitting the time course of the 500-ms fluorescence records ($\Delta F_{total}$) with a sum of two exponential functions, and ΔF versus voltage relations for medium and slow components were obtained. The $\Delta F_{med}$-V and $\Delta F_{slow}$-V were sigmoidal and were fitted by the Boltzmann relation (Fig. 3, C and D). $z\delta_F$ and $V_{0.5}^F$ were 0.8 and 3 mV (Fig. 3 C) for the medium, and 0.6 and 12 mV (Fig. 3 D) for the slow component. The mean values of the voltage sensitivity ($z\delta_F$) and midpoint voltage ($V_{0.5}^F$) from seven experiments were similar for both components: 0.9 ± 0.1 and −15 ± 3 mV for the medium, and 0.8 ± 0.1 and −17 ± 3 mV for the slow component.

The main difference between the medium and slow components was their amplitude. Maximal fluorescence change for the medium component ($\Delta F_{max}^{med}$) was 64 ± 1% ($n$ = 7) of the total maximal fluorescence change ($\Delta F_{total}^{max}$).

The dependence of the relaxation time constants for ΔF on voltage differed between medium and slow components. For medium, τ was 15 ± 1 ms at −150 mV and decreased to 8.7 ± 0.1 ms at +90 mV for ON (filled symbols, Fig. 3 E). For OFF, τ was independent of test voltage (open symbols, Fig. 3 E) and was 14.4 ± 0.3 ms ($n$ = 12). For slow ΔF (Fig. 3 F), τ (139 ± 8 ms, $n$ = 10) was relatively independent of voltage, for ON and OFF τ = 150 ± 14 ms.

### Part II. Presteady-State Kinetics in Sugar

Sugar increased the steady-state current (due to $Na^+$/sugar cotransport, see Fig. 1) and shifted the profile of the presteady-state currents. Fig. 4 A shows the total current records for the OFF-pulse when membrane potential was stepped from various test values ($V_t$, from +50 to −150 mV) back to the holding potential (−50 mV) from an oocyte in 0, 1, and 10 mM αMDG. The

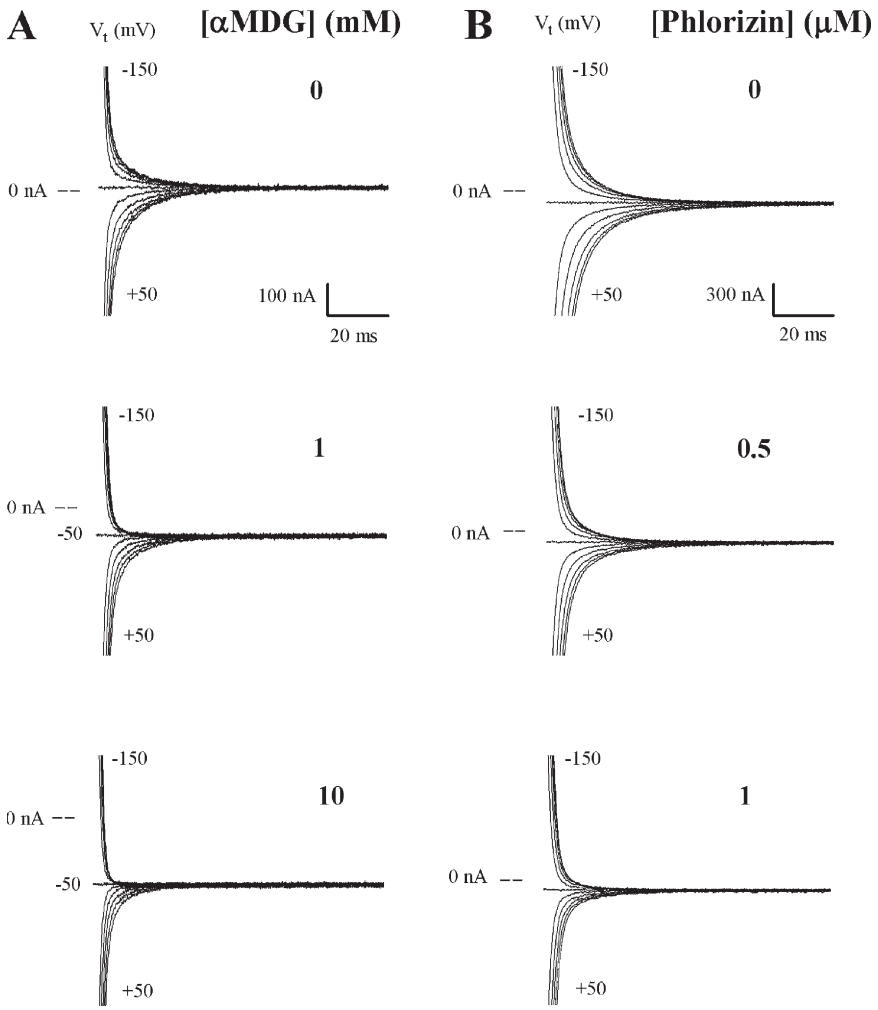


**Figure 4.** hSGLT1 G507C OFF currents in the presence of sugar (A) and phlorizin (B). Membrane potential was held at −50 mV ($V_h$), and shown are the selected total OFF current records (in response to a series of test voltage pulses from +50 to −150 mV) of an oocyte expressing G507C (unlabeled). The numbers beside the traces indicate the test voltage ($V_t$). (A) Effect of αMDG. OFF current records in $Na^+$ buffer (top), with 0.1 (middle) and 1 mM αMDG (bottom) added to the external solution. At $V_h$, the αMDG-induced currents were 14 and 99 nA at 0.1 and 1 mM αMDG. (B) Effect of phlorizin. OFF current records in $Na^+$ buffer, and with 0.5 and 1 μM phlorizin added to the external solution. Dashed lines represent zero current.

most pronounced effect of sugar was the reduction in presteady-state current with hyperpolarizing voltages. For example, at 10 mM $[\alpha MDG]_o$, the OFF currents for hyperpolarizing voltages was completely inhibited (Fig. 4 A). As in the absence of sugar, the ON and OFF charges were equal and opposite, and the Q-V relations at each $[\alpha MDG]_o$ fitted the Boltzmann relation (unpublished data). With increasing $[\alpha MDG]_o$ (from 0 to 100 mM), there was a reduction and eventual elimination in the maximal charge ($Q_{max}$) with a $K_{0.5}$ of 1.1 mM (Fig. 6 and Fig. 7 A). The midpoint voltage ($V_{0.5}$) shifted to more positive values (maximal shift was +60 mV, from −45 mV in NaCl alone to +15 mV in 10 mM αMDG) with a $K_{0.5}$ of 1.3 mM (Fig. 7 C). $z\delta_Q$ (=1.0) was unaffected by αMDG.

The fluorescence records were also dependent on αMDG (Fig. 5). As $[\alpha MDG]_o$ increased, the amplitudes of the fluorescence changes (ΔF) decreased at every test voltage, but in contrast to the presteady-state current, ΔF was not abolished at saturating $[\alpha MDG]_o$. This is illustrated in Fig. 6, which compares the current and fluorescence records in 100 mM $[\alpha MDG]_o$. Compared with the maximal fluorescence change ($\Delta F_{max}$) in NaCl buffer alone (Fig. 6 A), $\Delta F_{max}$ at 100 mM $[\alpha MDG]_o$ (Fig. 6 B) was only reduced 50%, whereas $Q_{max}$ was reduced more than 95%. The $K_{0.5}$ for the reduction in $\Delta F_{max}$ with $[\alpha MDG]_o$ was 1.1 ± 0.2 mM, and was similar to the $K_{0.5}$ for the reduction of $Q_{max}$ (Fig. 7 A). $V_{0.5}$ for ΔF shifted to more positive values with $[\alpha MDG]_o$. The $K_{0.5}$ (1.3 mM) was also similar to the $K_{0.5}$ for the shift of the $V_{0.5}$ for charge (Fig. 7 C). $z\delta_F$ (=0.8), as $z\delta_Q$ (=1.0), was unaffected by αMDG.

The relaxation time constants (τ) of the medium component of the presteady-state current showed a small decrease with increasing $[sugar]_o$, but only at hyperpolarizing voltages. For example, we determined τ in the presence and absence of 0.1 mM αMDG. In the case of G507C, there was no significant change in the ON and OFF time constants at either at +30 or −130 mV ($\tau_{ON}$ was 5.1 ± 0.4 at +30 mV, and 13.4 ± 0.6 ms at −130 mV, $n = 4$; and $\tau_{OFF}$ was 10.5 ± 0.4 ms, $n = 6$). For wild-type hSGLT1, there was also no significant change in $\tau_{ON}$ at +30 mV, but there was a reduction from 19 to 14 ms at −130 mV. At higher sugar concentrations we were unable to accurately determine the time constants of the medium component in the hyperpolarizing direction

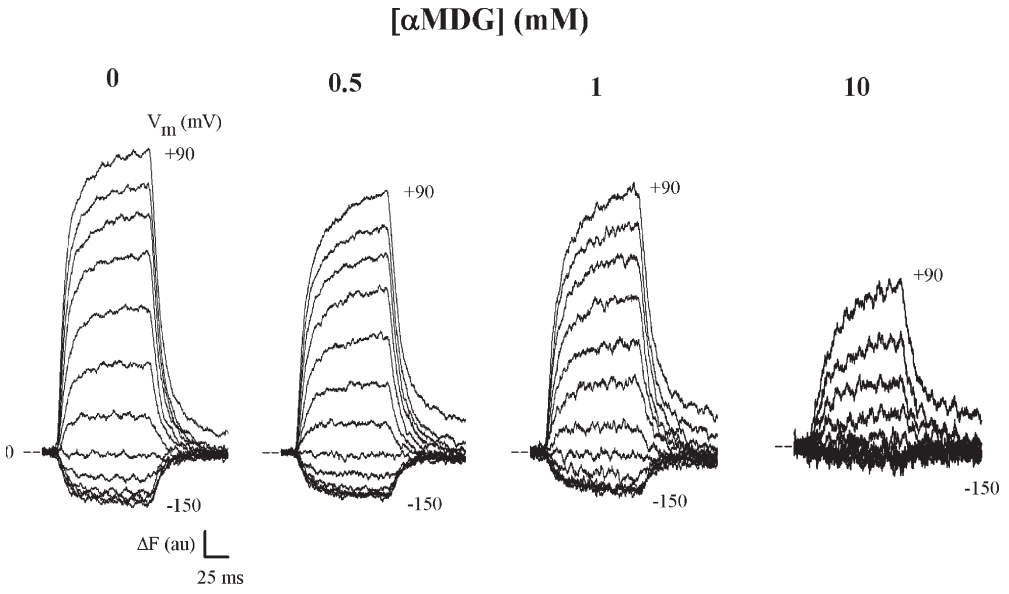


**Figure 5.** Effect of sugar on fluorescence. Time course of ΔF with step jumps in membrane voltage in NaCl buffer with various $[\alpha MDG]_o$ added (0, 0.5, 1, and 10 mM). Membrane potential was held at $V_h$ (−50 mV) and stepped to test values (from +90 to −150 mV) for 100 ms before returning to $V_h$. The dashed lines represent baseline fluorescence (ΔF = 0) at $V_h$. Abscissa and ordinate scales are the same for all panels. In this experiment, five $[\alpha MDG]_o$ were examined (0, 0.5, 1, 5, and 10 mM). Between each $[sugar]_o$, fluorescence records were obtained in sugar-free NaCl buffer to allow for compensation for photobleaching (Meinild et al., 2002). The apparent greater noise at 10 mM $[\alpha MDG]_o$ is due to the compensation for photobleaching.

or the slow component owing to the reduction of the presteady-state current (Fig. 7 A) and the positive shift in $V_{0.5}$ (Fig. 7 C).

The time constant (τ) of the medium component of ΔF was also unaffected by αMDG. On average, for ON, at +30 mV, τ was 10.7 ± 0.2 ms ($n$ = 5). At −150 mV, ΔF was too low for reliable estimates of τ (compare Fig. 5). On average, the time constant for OFF was 17.1 ± 0.3 ms ($n$ = 5). When large depolarizing voltages were applied at saturating sugar concentrations (>10 mM, compare Fig. 5 and Fig. 6 B), the time course of ΔF was slow, with τ ranging between 600 and 900 ms. In three experiments at 100 mM αMDG where 500-ms pulses were applied, the mean was 800 ± 100 ms.

### Blockade by Phlorizin

Phlorizin reduced, and at high concentrations eliminated, the presteady-state current, but did not alter the profiles of the OFF current records (Fig. 4 B). The maximal charge ($Q_{max}$) was reduced with $[phlorizin]_o$, with an inhibitory constant ($K_i$) of 0.3 μM (Fig. 7 B). There was no change in the $V_{0.5}$ (Fig. 7 D) and $z\delta_Q$ (not depicted)

Fig. 8 shows the effect of phlorizin on the fluorescence records. The inhibitor reduced ΔF at every test voltage. At the highest concentration applied (100 μM), ΔF was completely inhibited. The $K_i$ for the reduction of $\Delta F_{max}$ with $[phlorizin]_o$ was 0.4 μM, similar to the $K_i$ for the inhibition of charge (Fig. 7 B). There was also no effect of phlorizin on the $V_{0.5}$ (Fig. 7 D) and zδ for fluorescence (not depicted).

The time constants of the presteady-state current and ΔF were unaffected by phlorizin. For example, in the experiment of Fig. 4 B, as $[phlorizin]_o$ varied from 0 to 1 μM, on average, for the ON presteady-state currents at +50 and −150 mV, τ was 4.8 ± 0.3 ms ($n$ = 5) and 17.3 ± 0.4 ms ($n$ = 5), respectively. For OFF, on average, τ was 10.6 ± 0.3 ms ($n$ = 5). Likewise, in the experiment of Fig. 8, on average, for the ON fluorescence records at +30 mV, τ was 11.1 ± 0.2 ms ($n$ = 5). For OFF, τ was 14.6 ± 0.6 ms ($n$ = 5).

## DISCUSSION

The goal of this study is to examine sugar interactions with SGLT1 and to place this in context of a kinetic model for $Na^+$/sugar cotransport. We used a rhodamine-labeled mutant G507C of SGLT1 that transports sugar with similar kinetics as wild type. The kinetics of wild-type hSGLT1 and mutant G507C determined from the electrical and optical measurements (steady-state sugar-induced current, presteady-state current, and ΔF measurements) are summarized in Table I. Apart from the slight increase in $K_{0.5}^{\alpha MDG}$ for mutant G507C compared with wild-type hSGLT1 (1.7 vs. 0.3–0.5 mM), the kinetics of hSGLT1 are similar to those of the TMR6M-labeled G507C. The $K_{0.5}^{\alpha MDG}$ values were identical from electrical and optical measurements.

Our strategy was to perturb the steady-state distribution of conformations of the protein in the absence and presence of sugar or the competitive inhibitor phlorizin by step jumps in membrane voltage, and measure the presteady-state currents and changes in rhodamine fluorescence. The charge and fluorescence experiments provide insights into conformational changes induced

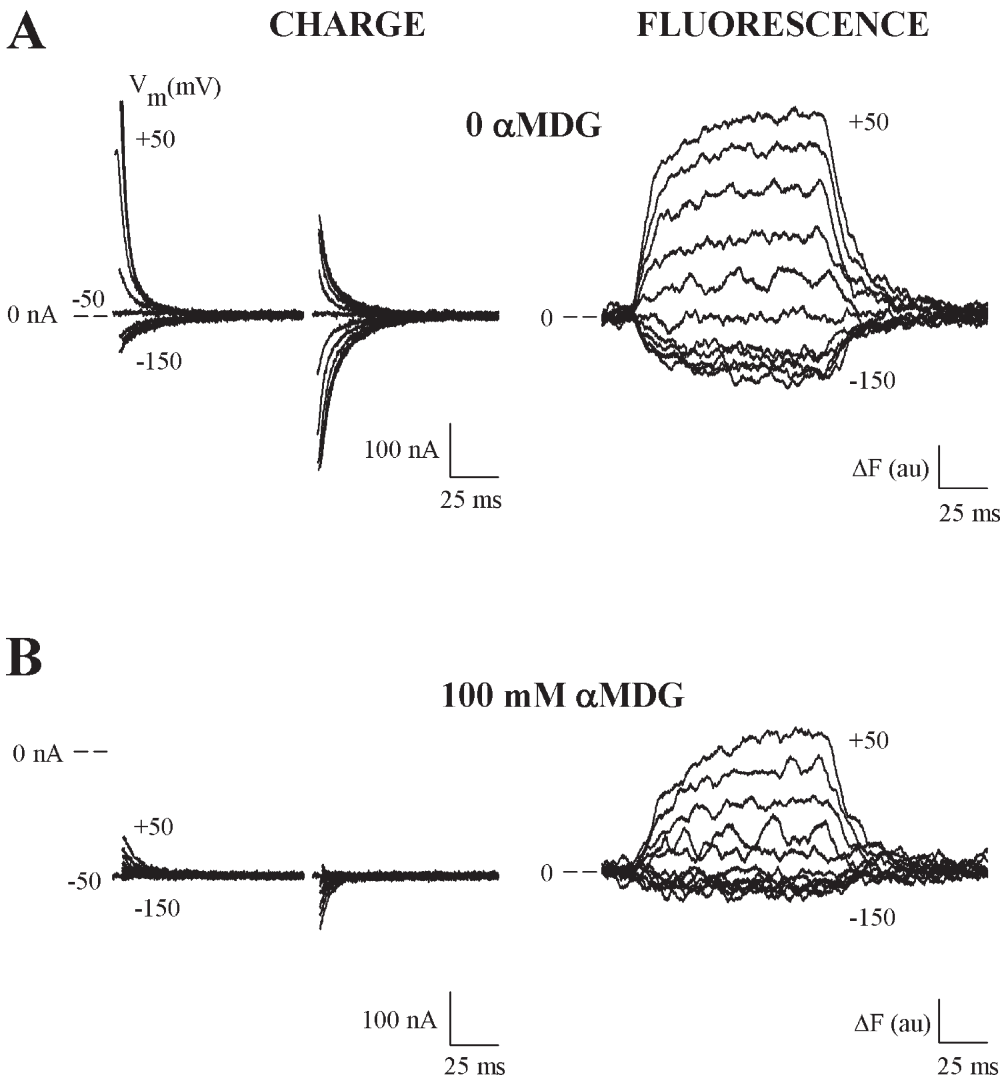


**Figure 6.** Comparison of charge and fluorescence (ΔF) records in the presence and absence of saturating $[\alpha MDG]_o$ (100 mM). Presteady-state current records for ON and OFF (compensated for oocyte membrane capacitance) and ΔF. $V_h$ was −50 mV and the test voltage varied from +50 to −150 mV. Numbers beside the traces are the test voltages. Dashed lines are the zero current or zero ΔF levels. (A) In NaCl buffer. (B) In NaCl buffer with 100 mM $[\alpha MDG]_o$.

by ligands ($Na^+$ and sugar) and membrane voltage. In the absence of sugar, we have previously shown that charge measurements, namely, the Q-V relations, are correlated with the steady-state distribution of hSGLT1 between conformations $C_2$ and $C_6$ ($C_2$ is the outward-facing $Na^+$-bound state, and $C_6$, the inward-facing empty transporter) (see Fig. 9 and Loo et al., 1998, 2005; Meinild et al., 2002). In addition, we have shown the fluorescence changes (ΔF) reflect differences in local environment of the fluorophore as the protein undergoes changes of conformations (Loo et al., 2005).

The key observations here are that αMDG and phlorizin reduce the presteady-state current and maximal fluorescence, and αMDG shifts the midpoint voltages ($V_{0.5}$) for charge and fluorescence. More importantly, at saturating $[\alpha MDG]_o$, presteady-state current was completely inhibited, whereas fluorescence change ($\Delta F_{max}$) was not (Fig. 6). The decrease in presteady-state current (and $Q_{max}$) is matched by the generation of the αMDG-induced steady-state current, i.e., $Na^+$/sugar cotransport (Loo et al., 1993). The reductions in $Q_{max}$ and $\Delta F_{max}$ and the shifts of the $V_{0.5}$'s with $[\alpha MDG]_o$ occurred with similar kinetics ($K_{0.5}^{\alpha MDG} \approx 1$ mM, Table I), indicating that they are all measurements of the same overall $Na^+$/glucose cotransport process. Phlorizin reduced $Q_{max}$ and $\Delta F_{max}$, but had no effect on $V_{0.5}$ (see also Hazama et al., 1997; Hirayama et al., 2001).

### Kinetic Model of SGLT1

Previously, we have developed and refined a model to account for the observed steady-state and presteady-state kinetics of SGLT1 (Parent et al., 1992b; Loo et al., 2002) Basically, this is a six-state, ordered, nonrapid equilibrium, alternating-access model with mirror symmetry and a $Na^+$/glucose transport stoichiometry of 2. We postulated that the ligand-free carrier is negatively charged (valence −2). There are six kinetic states, empty ($C_1$ and $C_6$), $Na^+$ bound ($C_2$ and $C_5$), and $Na^+$- and sugar-bound ($C_3$ and $C_4$) states in the external and internal membrane surfaces (Fig. 9). The $Na^+$ ions bind to the protein before glucose, and the substrates are transported simultaneously. To simplify the model we assumed the

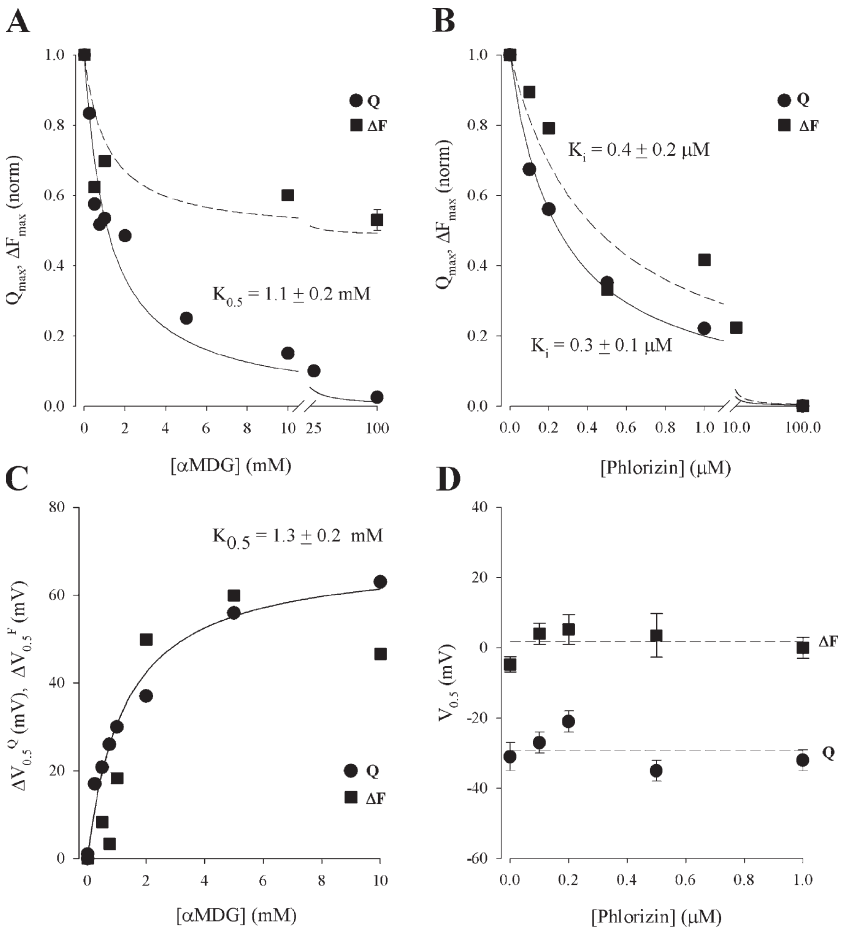


**Figure 7.** Effect of sugar and phlorizin on charge and fluorescence. (A) Dependence of $Q_{max}$ and $\Delta F_{max}$ on $[\alpha MDG]_o$. The line was the fit of the charge data to Eq. 1. The line through the ΔF data was drawn using Eq. 1 with a $K_{0.5}$ of 1.1 mM and a maximal change of 0.5 observed at 100 mM $[\alpha MDG]_o$. (B) Dependence of $Q_{max}$ and $\Delta F_{max}$ on $[phlorizin]_o$. The lines were fits of the data. (C) Dependence of the shift of $V_{0.5}$ for charge ($\Delta V_{0.5}^{Q}$) and fluorescence ($\Delta V_{0.5}^{F}$) on $[\alpha MDG]_o$. The line was obtained by fitting all the data. (D) Dependence of $V_{0.5}$ for charge and ΔF on $[phlorizin]_o$. The dashed lines represent the mean of the data points.

$Na^+$ ions bind to two identical $Na^+$ binding sites with the same rate constant. The only voltage-dependent steps are translocation of the ligand-free protein between the two sides of the membrane and the binding of external $Na^+$. The effects of voltage on these reaction steps were described by the Eyring rate theory. The presteady-state currents are associated with the voltage-dependent steps: binding of external $Na^+$ ($C_1 \rightleftarrows C_2$, 30% of total charge; Loo et al., 1993; Hazama et al., 1997) and translocation of the empty carrier ($C_1 \rightleftarrows C_6$, 70% of total charge).

All steady-state and presteady-state parameters (I/V curves, $K_{0.5}$ and $I_{max}$ values for $Na^+$ and sugar as a function of membrane voltage and given cis and trans concentrations) were computer generated simultaneously with numerical values assigned for the 12 of the 14 rate constants, and the results were compared

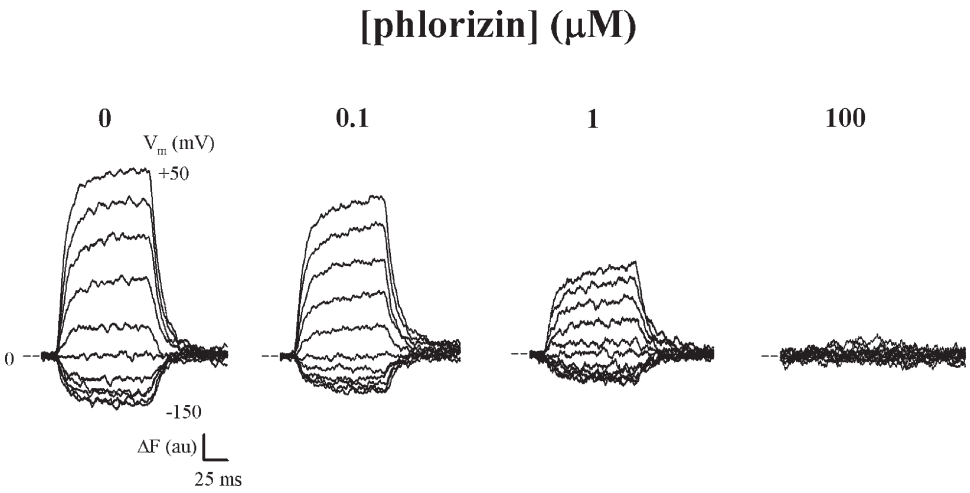


**Figure 8.** Effect of phlorizin on fluorescence. Shown is the time course of ΔF in NaCl buffer with $[phlorizin]_o$ (0, 0.1, 1, and 100 μM) in one oocyte. Membrane potential was held at $V_h$ −50 mV and stepped for 100 ms to $V_t$ (from +50 to −150 mV), before returning to $V_h$. Abscissa and ordinate scales are the same for all panels.

TABLE I

*Kinetic Parameters for Wild-type hSGLT1 and TMR6M-labeled hSGLT1 Mutant G507C*

| | Experimental | | | Simulation | |
|---|---|---|---|---|---|
| | G507C | G507C-TMR6M | hSGLT1 | G507C-TMR6M | hSGLT1 |
| Electrical | | | | | |
| Steady state | | | | | |
| $K_{0.5}^{\alpha MDG}$ (mM) | 1.7 ± 0.3 | 2.4 ± 0.3 | 0.30–0.49 [a,b] | 0.94 | 0.39 |
| $K_{0.5}^{Na}$ (mM) | 18 ± 1 | 25 ± 3 | 20–40 [a,c,d] | 16 | 16 |
| $K_i^{Pz}$ (nM) | ND | ND | 220 ± 70 [e] | 338 | 326 |
| Presteady-state | | | | | |
| $K_{0.5}^{\alpha MDG}$ (mM), $V_{0.5}$ shift | 1.6 ± 0.7 | 1.3 ± 0.2 | 0.16 ± 0.19 | 1.05 | 0.13 |
| $K_{0.5}^{\alpha MDG}$ (mM), $Q_{max}$ reduction | 1.1 ± 0.3 | 1.1 ± 0.8 | 0.21 ± 0.01 | 0.9 | 0.11 |
| $K_i^{Pz}$ (nM), $Q_{max}$ reduction | 180 ± 24 | 250 ± 39 | 200 ± 23 | 277 | 277 |
| Optical | | | | | |
| $K_{0.5}^{\alpha MDG}$ (mM), $V_{0.5}$ shift | – | 1.3 ± 0.2 | – | 1.1 | – |
| $K_{0.5}^{\alpha MDG}$ (mM), $\Delta F_{max}$ reduction | – | 1.1 ± 0.8 | – | 0.5 | – |
| $K_i^{Pz}$ (nM), $Q_{max}$ reduction | – | 450 ± 250 | – | 399 | – |

Steady-state kinetic parameters (Experimental and Simulation) were all obtained at $V_m = -50$ mV. Simulations were performed on the eight-state kinetic model for wild-type hSGLT1 and mutant G507C using the kinetic parameters listed in Table II. $K_{0.5}^{\alpha MDG}$ and $K_{0.5}^{Na}$ from steady-state measurements on G507C and G407C-TMR6M are the mean ± SEM of three to seven experiments. ND, not determined. Statistics shown for $K_{0.5}^{\alpha MDG}$, $K_{0.5}^{Na}$, and $K_i^{Pz}$ from presteady-state and optical measurements are the errors of the fit for individual oocytes, but these were repeated on at least three oocytes.

[a]Hirayama et al., 1996.

[b]Diez-Sampedro et al., 2000.

[c]Loo et al., 2000.

[d]Quick et al., 2001.

[e]Hirayama et al., 2001.

and contrasted with the experimental datasets. Optimization of the simulations was accomplished by progressively adjusting each rate constant to obtain a global fit to the experimental results. A single set of rate constants, reasonable but not necessarily unique, was obtained that accounted for the overall behavior of the cotransporter, including the I/V curves in the presence and absence of sugar, the steady-state kinetics of inward $Na^+$/sugar cotransport as a function of the external ligand concentrations and voltage (Parent et al., 1992b).

Subsequently, we tested and refined the model by detailed investigations of: (a) the presteady-state behavior of SGLT1 as a function of external $Na^+$ concentration, membrane voltage, and temperature (Loo et al., 1993, 2005, Hazama et al., 1997); (b) the stoichiometry of $Na^+$ and glucose cotransport (Mackenzie et al., 1998); (c) $Na^+$ transport in the absence of substrate (Loo et al., 1999); (d) the kinetics of reverse $Na^+$/glucose cotransport (Quick et al., 2003; Eskandari et al., 2005); (e) the conformational states of SGLT1 as a function of ligand concentrations and membrane voltage using optical techniques on a TMR6M-labeled hSGLT1 mutant (Q457C) where $Na^+$/sugar cotransport is abolished after labeling (Loo et al., 1998, 2005; Meinild et al., 2002) and (f) electron microscopic techniques to determine the density of SGLT1 in the membrane (Zampighi et al., 1995). These comprehensive studies support the validly of the model but require the presence of two additional states ($C_a$ and $C_b$) between $C_1$ and $C_6$ to account for the presteady-state behavior (shaded region of Fig. 9; Loo et al., 2005). The major discrepancies between the model and the observed behavior are the fast presteady-state kinetics in the submillisecond range, and these are thought to be due to assumptions about $Na^+$ binding to two identical sites with similar rate constants (see Loo et al., 2005 and below). In this study we have employed the eight-state model (Fig. 9) along with electrical and optical methods to examine the conformational states during the $Na^+$/glucose cotransport cycle. Since the binding of the high-affinity inhibitor phlorizin is $Na^+$ dependent, this is incorporated into the model as $C_2 \rightleftharpoons C_7$ ($[CNa_2]' + Pz \rightleftharpoons [CNa_2Pz]'$) with ON and OFF rates $k_{27}$ and $k_{72}$ (Fig. 9). Phlorizin binding to the cytosolic surface of SGLT1 ($[CNa_2]'' + Pz \rightleftharpoons [CNa_2Pz]''$) is neglected owing to the low affinity ($K_i > 1$ mM; Quick et al., 2003; Eskandari et al., 2005).

### Model Simulations

As a starting point, we used the rate constants for the voltage-dependent steps from Loo et al. (2005). The rate constants for the sugar binding and translocation steps ($k_{23}$, $k_{32}$, $k_{34}$, and $k_{43}$) are from Hirayama et al. (1996). The rate constants for $Na^+$ and sugar binding on the internal membrane are from Eskandari et al. (2005). We extend the model to mutant G507C by reducing the rates for sugar binding ($k_{23}$, $k_{54}$) for mutant G507C to account for the lower $K_{0.5}^{\alpha MDG}$ (Table I). A set

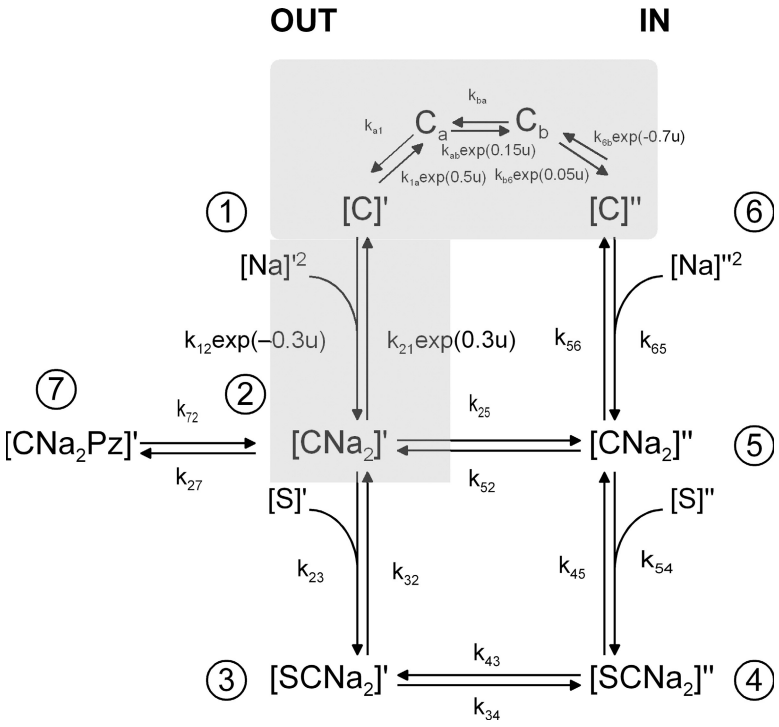


**Figure 9.** An eight-state kinetic model for SGLT1. This model is an extension of the six-state model proposed by Parent et al. (1992b) with inclusion of intermediate states ($C_a$ and $C_b$) between $C_1$ and $C_6$ (Loo et al., 2005). Kinetic states of the transporter consist of the empty transporter C (states $C_1$ and $C_6$), $Na^+$-bound $CNa_2$ (states $C_2$ and $C_5$), $Na^+$- and sugar-bound $SCNa_2$ (states $C_3$ and $C_4$) in the external (′) and internal membrane surfaces (″). Two $Na^+$ ions bind to the protein before the sugar molecule. The shaded region represents the voltage-dependent steps: conformational change of the empty transporter between the external and internal membrane surfaces ($C_1 \rightleftarrows C_a \rightleftarrows C_b \rightleftarrows C_6$), and $Na^+$ binding/dissociation ($C_1 \rightleftarrows C_2$). Rate constants ($k_{ij}$) for transitions between states ($C_i \rightarrow C_j$) are $k_{ij} = k_{ij}^o \exp(-\varepsilon_{ij}FV/RT)$, where $k_{ij}^o$ is a voltage-independent rate, $\varepsilon_{ij}$ is the equivalent charge movement, and F, R, and T have their usual physicochemical meanings (see Simulation of SGLT1 in Materials and methods). In Fig. 9, the reduced membrane voltage u = FV/RT. The rate constants obey the microscopic reversibility conditions (compare Parent et al., 1992b): $k_{52}^o\, k_{21}^o\, k_{1a}^o\, k_{ab}^o\, k_{b6}^o\, k_{65}^o = k_{12}^o\, k_{25}^o\, k_{56}^o\, k_{6b}^o\, k_{ba}^o\, k_{a1}^o$, and $k_{54}^o\, k_{43}^o\, k_{32}^o k_{25}^o = k_{45}^o\, k_{52}^o\, k_{23}^o\, k_{34}^o$.

of rate constants was obtained (Table II) that accounts qualitatively and quantitatively for the steady-state and presteady-state experimental data (see below). As a working hypothesis we assume that changes in fluorescence intensity (ΔF) associated with SGLT1 were due to differences in apparent quantum yield of the bound fluorophore in different conformations: $\Delta F \approx q_{y1}\Delta C_1 + q_{y2}\Delta C_2 + q_{y3}\Delta C_3 + q_{y4}\Delta C_4 + q_{y5}\Delta C_5 + q_{y6}\Delta C_6 + q_{ya}\Delta C_a + q_{yb}\Delta C_b$. This hypothesis is supported by the findings that in the SGLT homologue (vSGLT) from *Vibrio parahaemolyticus* (Veenstra et al., 2004), and hSGLT1 mutant Q457C (unpublished data), the sugar-induced quenches of fluorescence of covalently linked extrinsic fluorophores are not accompanied by shifts in absorption or emission spectra. As discussed below, since the occupancy probabilities of conformations $C_1$, $C_3$, $C_4$, $C_a$, and $C_b$ are negligible, the fluorescence signal is reduced to $\Delta F \approx q_{y2}\Delta C_2 + q_{y5}\Delta C_5 + q_{y6}\Delta C_6$.

*Steady-State Kinetics.* The eight-state model accounted quantitatively for the kinetics of steady-state $Na^+$/glucose cotransport as a function of extracellular ligand concentrations and voltage (Table I). The sugar-induced currents increased and saturated with hyperpolarizing voltages (compare Fig. 1 C). The simulated $K_{0.5}$ for αMDG and $Na^+$ ($K_{0.5}^{\alpha MDG}$, $K_{0.5}^{Na}$) decreased with hyperpolarizing voltages. Between −50 and −150 mV, $K_{0.5}^{Na}$ decreased from 16 to 3 mM, and $K_{0.5}^{\alpha MDG}$ decreased from 0.39 to 0.24 mM (unpublished data). The model also simulated the kinetics of reverse cotransport as a function of intracellular ligand concentrations (unpublished data; see Eskandari et al., 2005).

*Occupancy Probabilities.* Ligands and voltage alter the occupancy probability ($P_o$) of each state (Fig. 10 A). In external NaCl buffer, the transporter is predominantly in $C_2$ at negative membrane voltages (98% occupancy in $C_2$ at −150 mV), and in $C_6$ at positive voltages (e.g., 73% in $C_6$ at +50 mV). External sugar alters the distribution by reducing the occupancy in $C_2$ and increasing $C_5$ occupancy at large negative membrane voltages. At large positive voltages (e.g., +50 mV), $C_6$ is predominant, regardless of $[sugar]_o$ (Fig. 10, A, B and D). For example, at 10 mM $[\alpha MDG]_o$, $C_5$ is the highest occupancy state (57%) at $V_m$ −150 mV, and $C_6$ (69%) at $V_m$ +50 mV.

This analysis predicts large changes in the distribution of SGLT1 with jumps in membrane potential, and for the voltage-dependent transitions, a presteady-state current.

*Presteady-State Kinetics.* Fig. 11 A shows the simulated presteady-state currents for the OFF-pulses in response to the standard 100-ms voltage pulse protocol ($V_h$ = −50 mV; compare Fig. 1 A). The currents are progressively reduced with increasing $[sugar]_o$, and at 10 mM, they are inhibited 82% (Fig. 11 D). The simulated Q-V relations for medium change (at each $[sugar]_o$) could be fitted by Boltzmann relations. Without sugar, $V_{0.5}$ = −32 mV and $z\delta_Q = 0.9$. Increasing $[sugar]_o$ reduced the maximal charge ($Q_{max}$) with a $K_{0.5}^{\alpha MDG}$ of 0.9 mM (Table I). Sugar also shifted the midpoint voltage ($V_{0.5}$) to more positive values, with a simulated $K_{0.5}$ of 1.1 mM (maximal shift was +56 mV). These are close to the experimentally measured $K_{0.5}^{\alpha MDG}$ of 1.1 and 1.3 mM (Table I).

The τ-V relations are simulated by the model. In the absence of sugar, there are four time constants, two fast ($\tau_{fast} < 1$ ms), one medium ($\tau_{med}$ 3–25 ms), and a slow ($\tau_{slow}$ 30–100 ms; Loo et al., 2005). $\tau_{med}$ and $\tau_{slow}$ are voltage independent for hyperpolarizing voltages and decreased with depolarizing voltages (see Fig. 16 C of Loo et al., 2005). Simulations indicate that the time constant $\tau_{med}$ for ON (as $V_m$ is stepped from −50 to +50 mV) is relatively unaffected at $[sugar]_o$ below the $K_{0.5}$; e.g., at +50 mV, $\tau_{ON}$ decreased by <1 ms when $[sugar]_o$ increased from 0 to 1 mM. Experimentally, we found in the range 0–1 mM, the time constant (at $V_t$ = 30 mV) was independent of $[\alpha MDG]_o$ (see Results). The simulations indicated a decrease in $\tau_{med}$ (by ≈5 ms) in the hyperpolarizing direction. However, since the presteady-state current in response to hyperpolarizing voltage pulses was abolished by external sugar (see Fig. 1, A and B), accurately resolving this difference is beyond the resolution of the method.

*Fluorescence.* There is good agreement between our model simulations and the experimental data as functions of voltage and the concentrations of sugar and phlorizin (Fig. 12). In the presence of 100 mM external $Na^+$, the ON responses for 100-mV jumps in membrane potential from −50 mV to +50 and −150 mV matched the experimental observation in the presence and absence of external sugar (0, 1, and 10 mM) in terms of (a) the magnitude of the changes in fluorescence; (b) the asymmetry of the response to depolarizing and hyperpolarizing voltage steps; and (c) the reduction in ΔF with increasing $[sugar]_o$ (Fig. 12). These fits were within the normal variation recorded from experiment to experiment. A discrepancy between the simulations and the data is in the relative magnitude of the fast and medium components for the OFF responses when the test voltage returned from +50 mV to the holding potential. The underestimated size of the fast component is likely to be due to our simplifying assumptions about $Na^+$ binding (see below).

We also simulated ΔF as a function of membrane potential in the presence and absence of sugar and phlorizin (Fig. 13) to obtain the presteady-state parameters $\Delta F_{max}$, $V_{0.5}$, and $z\delta_F$ as functions of sugar and phlorizin concentrations. The ΔF-V relations saturated at −150 and +90 mV and fitted the Boltzmann relation (with a $z\delta_F$ of 0.7 and $V_{0.5}$ of −11 mV). With saturating sugar (10 mM αMDG), $\Delta F_{max}$ was reduced by 53%, with a $K_{0.5}$ of 0.5 mM (Table I). $V_{0.5}$ also shifted with increasing $[sugar]_o$ (maximum shift was +51 mV) with a $K_{0.5}$ of 1.1 mM (Table I). Thus the observed small reduction of $\Delta F_{max}$ (≈50%) compared with $Q_{max}$ (>95%, Fig. 6 B) is reproduced by the simulations.

In the absence of sugar, with a large depolarizing voltage pulse (e.g., from −50 to +50 mV), the fluorescence changes are due to the transition $C_2 \rightarrow C_6$ (Fig. 10 A), as the voltage jump dictates a new equilibrium state distribution highly favoring $C_6$ (Fig. 14 C; see also Fig. 10 A). Thus the apparent quantum yield of $C_6$ must be higher than that of $C_2$, as there is an increase in ΔF (Figs. 3 and 13). This series of conformational changes involve all the voltage-dependent transitions (Fig. 9, shaded region). On the other hand, at saturating $[\alpha MDG]_o$ (e.g., 10 mM; Fig. 10 D), $C_5$ is the most highly populated state at $V_h$ (−50 mV), and a depolarizing voltage favors $C_6$ over $C_5$ (see Fig. 10 D and Fig. 14 D). So if the quantum yield of $C_6 > C_5$, on depolarization, we would observe an increase in ΔF (Fig. 14 B). The

TABLE II

*Rate Constants and Parameters for the Eight-State Kinetic Model for hSGLT1 and Mutant G507C*

| | | | |
|---|---|---|---|
| $k_{12}$ = 140,000 $M^{-2}s^{-1}$ | $k_{21}$ = 300 $s^{-1}$ | $\varepsilon_{12}$ = 0.3 | $\varepsilon_{21}$ = 0.3 |
| $k_{1a}$ = 600 $s^{-1}$ | $k_{a1}$ = 35 $s^{-1}$ | $\varepsilon_{1a}$ = 0.5 | $\varepsilon_{a1} \approx 0$ |
| $k_{ab}$ = 20 $s^{-1}$ | $k_{ba}$ = 15 $s^{-1}$ | $\varepsilon_{ab}$ = 0.15 | $\varepsilon_{ba} \approx 0$ |
| $k_{b6}$ = 300 $s^{-1}$ | $k_{6b}$ = 300 $s^{-1}$ | $\varepsilon_{b6}$ = 0.05 | $\varepsilon_{6b}$ = 0.7 |
| $k_{34}$ = 50 $s^{-1}$ | $k_{43}$ = 50 $s^{-1}$ | | |
| $k_{56}$ = 5 $s^{-1}$ | $k_{65}$ = 2,250 $M^{-2}s^{-1}$ | | |
| $k_{25}$ = 0.01 $s^{-1}$ | $k_{52} = 4.5 \times 10^{-4} s^{-1}$ | | |
| hSGLT1 | | | |
| $k_{23}$ = 45,000 $M^{-1}s^{-1}$ | $k_{32}$ = 20 $s^{-1}$ | | |
| $k_{54}$ = 81,667 $M^{-1}s^{-1}$ | $k_{45}$ = 800 $s^{-1}$ | | |
| hSGLT1 G507C-TMR6M | | | |
| $k_{23}$ = 8,000 $M^{-1}s^{-1}$ | $k_{32}$ = 20 $s^{-1}$ | | |
| $k_{54}$ = 14,518 $M^{-1}s^{-1}$ | $k_{45}$ = 800 $s^{-1}$ | | |
| $\varphi_5/\varphi_2$ = 3 | $\varphi_6/\varphi_2$ = 6 | | |
| $\varphi_1$, $\varphi_a$, $\varphi_b$, $\varphi_3$, $\varphi_4$ | indeterminate | | |
| Phlorizin binding/dissociation | | | |
| $k_{27}$ = 50,000 $M^{-1}s^{-1}$ | $k_{72}$ = 0.01 $s^{-1}$ | | |

The rate constants were obtained by interactive numerical simulations of the model (Fig. 9) and were evaluated by visual goodness-of-fit to the observed global kinetic behavior of hSGLT1 (including steady-state and presteady-state kinetics, i.e., current–voltage (fluorescence–voltage) curves and apparent affinities and maximum values for currents and TMRM fluorescence as functions of cis and trans $Na^+$, sugar, and phlorizin concentrations (see Parent et al., 1992b). As a starting point we used the parameters obtained for rabbit SGLT1 (Parent et al., 1992b) and the rates $k_{52}$ and $k_{54}$ were chosen as the dependent parameters (imposed by microscopic reversibility). The values for rate constants involved in sugar binding and transport, $k_{32}$, $k_{34}$, $k_{43}$, and $k_{45}$, were unchanged from Parent et al. (1992b), while $k_{23}$ was varied according to the $K_{0.5}$ for inward sugar transport by hSGLT (0.3–3 mM, Hirayama et al., 1996, and present study). The rates for $Na^+$ and sugar binding at the internal surface, $k_{54}$, $k_{56}$, and $k_{65}$, were revised after recording the kinetic parameters for reverse $Na^+$/sugar cotransport (Quick et al., 2003; Eskandari et al., 2005). The voltage-dependent rate constants ($k_{12}$, $k_{21}$, $k_{1a}$, $k_{a1}$, $k_{ab}$, $k_{ba}$, $k_{b6}$, and $k_{6b}$) were taken from Loo et al. (2005). The magnitude of SGLT1 $Na^+$-uniport, i.e., SGLT1-mediated $Na^+$ transport in the absence of sugar, limits the value of $k_{25}$. The rates for phlorizin association and dissociation, $k_{27}$ and $k_{72}$, are determined by the phlorizin inhibitory constant (0.2–0.4 μM) and $k_{72} < 0.01$ $s^{-1}$, the insignificant release of phlorizin when the membrane potential jumped to +50 mV for up to 2 s. For detailed discussion on the evaluation of these rate constants see Parent et al. (1992b) and Loo et al. (2005). The quantum yields ($\varphi_j$) for TMRM6-G507C-hSGLT1 were also obtained by numerical simulations.

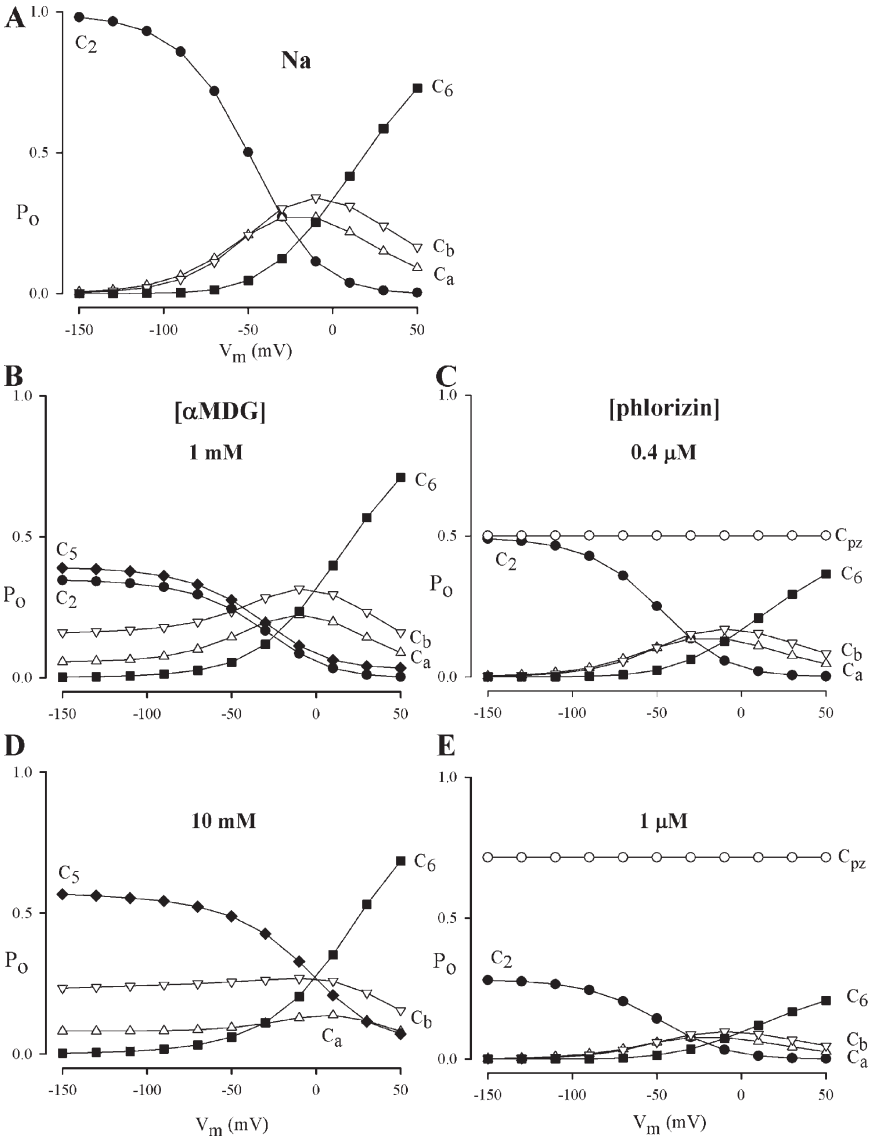


**Figure 10.** Simulation predictions on occupancy probabilities ($P_o$). The simulations were performed in 100 mM external $Na^+$. A, B, and D show $P_o$ as a function of voltage in the presence of 0, 1, and 10 mM $[\alpha MDG]_o$. C and E show the distribution of conformations in the presence of external phlorizin (0.4 and 1 μM). $C_{pz}$ is the phlorizin-bound state $[CNa_2Pz]'$. For clarity, states with occupancy probabilities $<0.1$ were not plotted. The states were as follows: $C_1$ in A, C, and E; and $C_1$, $C_2$, $C_3$, and $C_4$ in B and D.

change in ΔF is slower than in $Na^+$ alone (Fig. 14 A), as is observed experimentally (Figs. 5 and 12). The charge movements arising from the concurrent relaxation of the voltage-dependent transitions (shaded region, Fig. 9) are negligible, owing to the negligible occupancy of $C_2$ at $V_h$ (Fig. 10).

*Effect of Phlorizin.* Phlorizin locked the transporters in fixed state ($C_7$ in Fig. 9) and prevented the protein from running through the transport cycle. This is illustrated by the occupancy probabilities as $[phlorizin]_o$ is varied. The increase in the occupancy of the phlorizin-bound state ($[CNa_2Pz]'$) is balanced by reduction of the occupancy probabilities ($P_o$) in the other conformations (Fig. 10, A, C, and E). The profile of the $P_o$-$V_m$ curves is not affected by phlorizin. The simulated inhibitory constant ($K_i^{Pz}$) for phlorizin inhibition of the sugar-induced current from Dixon analysis is 338 nM, compared with the observed value of 220 ± 70 nM (Table I). At the $K_i^{Pz}$, 50% of the transporters are in the phlorizin-bound conformation ($[CNa_2Pz]'$, Fig. 10 C).

The effects of phlorizin on presteady-state currents and fluorescence (ΔF) is simulated in Fig. 11 (C and E) and Fig. 13 (C and E) for 0.4 and 1 μM phlorizin. The amplitudes of the presteady-state current and ΔF are reduced at every test voltage. Analysis of the Q-V and ΔF-V relations as $[phlorizin]_o$ was varied from 0 to 100 μM showed that maximal charge ($Q_{max}$) and maximal fluorescence ($\Delta F_{max}$) were reduced by phlorizin, with $K_i$'s of 277 nM for charge and 399 nM for fluorescence. There were no changes in the $V_{0.5}$ (and zδ) values for both charge and fluorescence.

Our estimate of the rate constants for phlorizin binding and dissociation for human SGLT1 ($k_{27}$ = 50,000 $M^{-1}s^{-1}$, $k_{72}$ = 0.01 $s^{-1}$) was obtained with the requirements that (a) the ratio $k_{72}/k_{27}$ is the dissociation constant $K_D$ ($K_D$ = $k_{72}/k_{27}$ = 0.2 μM from Dixon analysis; Panayotova-Heiermann et al., 1995; Hirayama et al., 2001), and

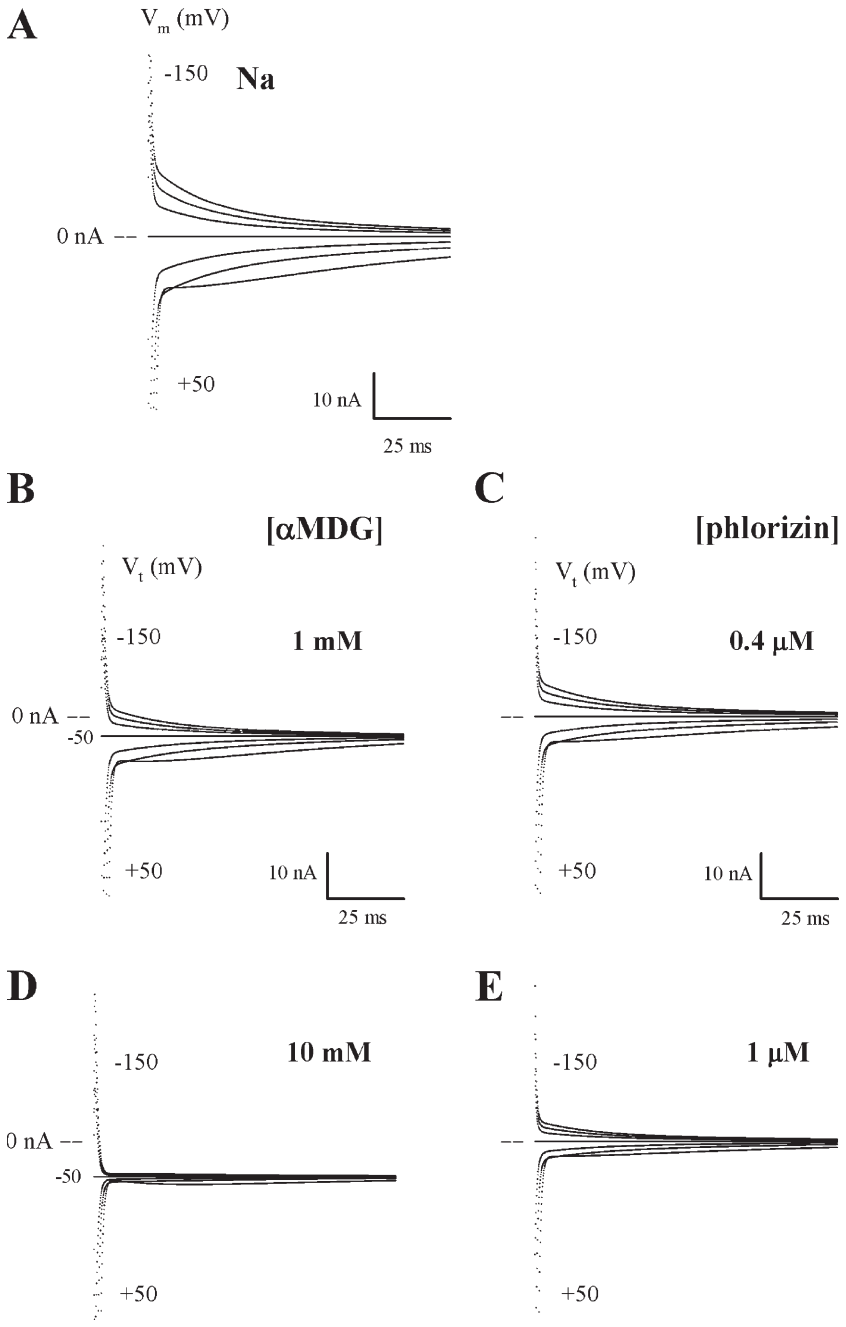


**Figure 11.** Simulated OFF currents. The simulations were performed in 100 mM external $Na^+$. (A, B, and D) OFF currents with 0, 1, and 10 mM αMDG in the external medium. (C and E) OFF currents in the presence of 0.4 and 1 μM external phlorizin. $V_h$ was −50 mV, and currents shown (for test voltages at +50, +10, −30, −50, −70, −90, and −150 mV) have been filtered at 500 Hz. Using the cut-open oocyte voltage clamp, we have previously found that there are two fast components of presteady-state currents with time constants of 0.18 and 1.3 ms (Loo et al., 2005). In the two-electrode voltage clamp, they are hidden by the oocyte membrane capacitance.

(b) the phlorizin-bound state ($[CNa_2Pz]'$) does not decay significantly during 2-s depolarizing voltage pulses. These estimates are within the range of values obtained previously by Toggenburger et al. (1982) on rabbit small-intestinal brush border membrane vesicles: $k_{27} \approx 18{,}000$–$150{,}000\ M^{-1}s^{-1}$, $k_{72} = 0.4\ s^{-1}$, and $K_D = 2.7\ \mu M$.

### Simulation Conclusions

(a) We have obtained a single set of kinetic parameters that accounts for the global experimental observations on steady-state and presteady-state kinetics, for both charge and fluorescence measurements in the presence and absence of sugar or phlorizin.

(b) In view of the close agreement between the data and simulations on charge movements in the presence of sugar, this suggests that there are no significant voltage-dependent steps in the transport cycle other than those associated with external $Na^+$ binding/dissociation and conformational change of the empty transporter (shaded region of Fig. 9). This is in agreement with our previous study on reverse $Na^+$/sugar cotransport using the giant patch (Eskandari et al., 2005).

(c) At saturating $[\alpha MDG]_o$, when membrane voltage is stepped from −50 to +50 mV, the charge movement is too small to be detected because of the low occupancy in states $C_2$, $C_1$, $C_a$, $C_b$, and $C_6$ (Fig. 10 D and

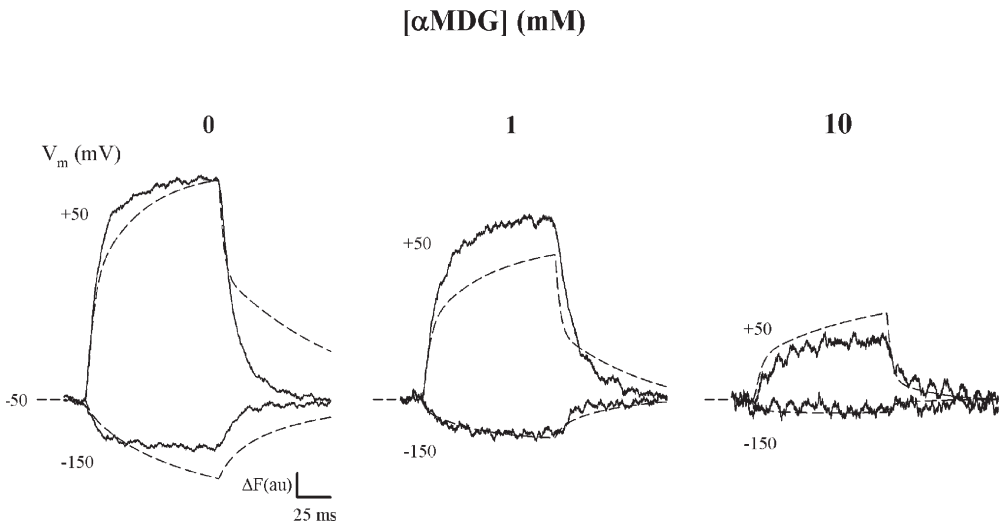


**Figure 12.** Comparison of fluorescence data and simulation of the eight-state model (Fig. 9). Simulation was performed using the kinetic parameters of Table II. Representative fluorescence traces at test voltages +50 and −150 mV from $V_h$ (−50 mV) are from Fig. 5. The dashed lines are the simulated ΔF. The apparent quantum yields used for the simulation were $q_2 = 1$, $q_6 = 5$, and $q_1 = q_a = q_b = q_3 = q_4 = q_5 = 3$. Abscissa and ordinate scales are the same for all panels.

Fig. 14 D), which is observed experimentally (Fig. 6 B). However, there is a fluorescence change (bold line of Fig. 14 B) due to the transition: $C_5 \rightarrow C_6$ (bold lines in Fig. 14 D). This is a rate-limiting step for $Na^+$/sugar cotransport, and we have thus experimentally isolated a conformational change that has not been previously described. The differential sensitivities of the electrical and optical measurements allow us to measure the fluorescence change associated with the electroneutral steps.

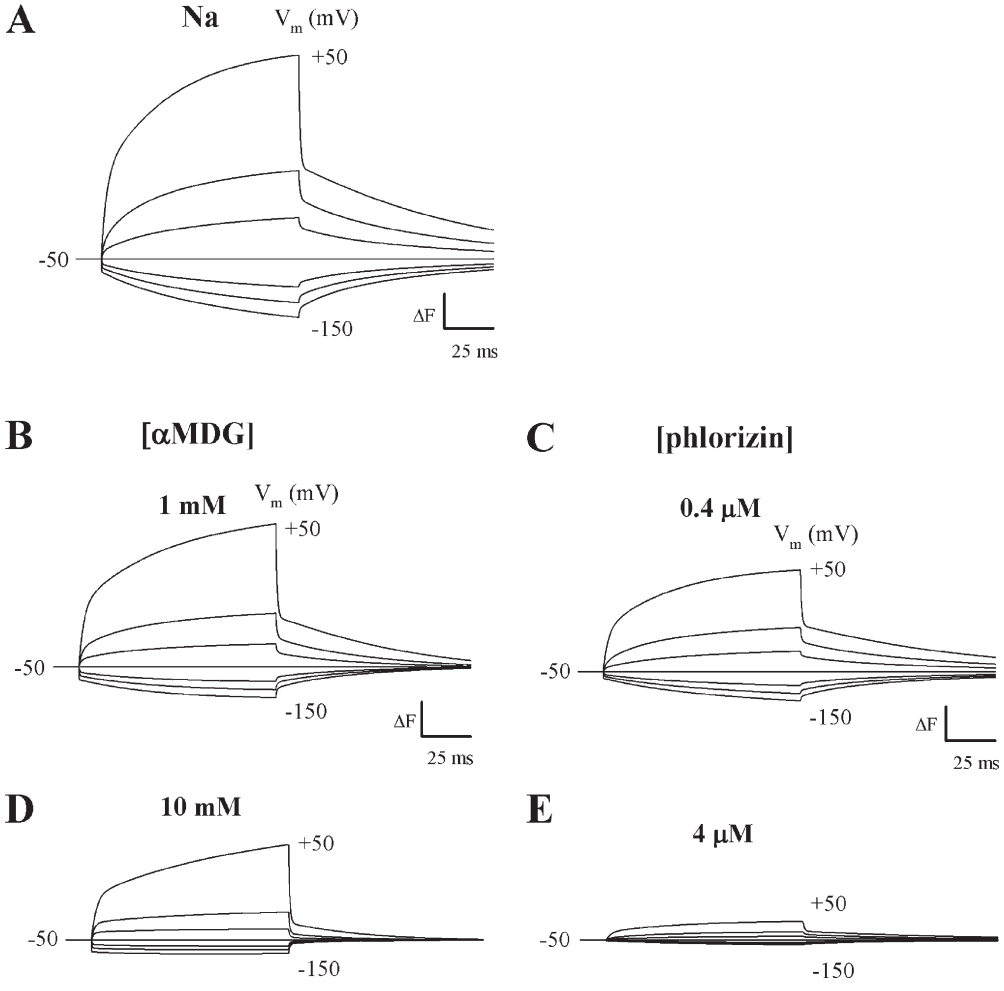


**Figure 13.** Simulated fluorescence records. The simulations were performed in 100 mM external $Na^+$. (A, B, and D) Time course of fluorescence intensity change (ΔF) with 0, 1, and 10 mM αMDG in the external solution. (C and E) Effect of phlorizin (0.4 and 4 μM). Total fluorescence (F) associated with SGLT1 is defined by $F \approx q_1C_1 + q_2C_2 + q_aC_a + q_bC_b + q_3C_3 + q_4C_4 + q_5C_5 + q_6C_6$, where $q_j$ is the apparent quantum yield of the fluorophore (TMR6M) when SGLT1 is in conformation $C_j$. Fluorescence records were simulated with $q_1 = 3$, $q_2 = 1$, $q_a = 3$, $q_b = 3$, $q_4 = 3$, $q_5 = 3$, $q_6 = 6$. Shown are the predicted ΔF records when $V_m$ is stepped from −50 mV to $V_t$ (+50, +10, −30, −50, −70, −90, and −150 mV). Steady-state fluorescence levels have been removed. The simulation for ΔF in the presence of phlorizin is independent of the quantum yield of the phlorizin-bound state ($[CNa_2Pz]'$). See Table I for comparison of simulated and observed presteady-state kinetic parameters.

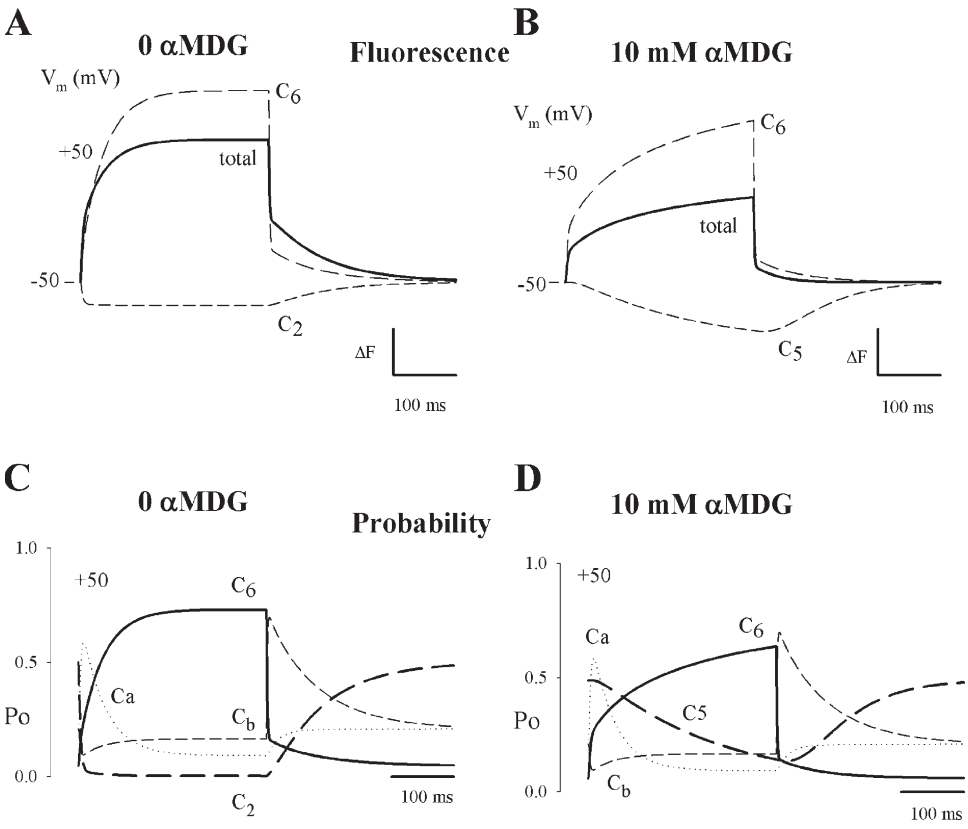


**Figure 14.** Simulated conformational change C5≡C6. The simulations were performed with 300-ms voltage pulses in 100 mM external $Na^+$. (A and B) Components of fluorescence change (ΔF) when $V_m$ was stepped from −50 to +50 mV with 0 and 10 mM αMDG in the external solution. The bold lines are the total ΔF, and the broken lines are changes of fluorescence due to $C_2$, $C_5$, and $C_6$. (C and D) Time course of occupancy probability ($P_o$) in 0 and 10 mM αMDG.

(d) Simulations show that the model accounts for the reductions in the $Q_{max}$ and $\Delta F_{max}$ and the shifts in $V_{0.5}$ for charge and fluorescence produced by external sugar (or phlorizin). While the apparent valence ($z\delta$) is similar for both charge movement and fluorescence changes ($z\delta \sim 0.7$–$0.9$), this may depend on the nature and position of the fluorophore and its local interactions with SGLT1. The apparent valence ($z\delta_Q$) for charge movement is the sum ($=z_1\delta_1 + z_2\delta_2 + .. + z_n\delta_n$) of the products of moveable charges ($z_i$) and the displacement ($\delta_i$) of each charge in the membrane electric field, whereas the apparent valence ($z\delta_F$) for fluorescence depends on the apparent quantum yields of the fluorophore in different protein conformations. While the apparent valence of SGLT1 and mutant charge movement have been found to be 1, the observed values of $z\delta_F$ varied: $z\delta_F = 0.4$ for TMR6M-Q457C (Loo et al., 1998, 2005; Meinild et al., 2002), 0.7 for TMR6M-D454C (Diez-Sampedro et al., 2004), and 0.9 for TMR6M-G507C (this study).

(e) The previous six-state model could account for the steady-state kinetics of SGLT1 and the steady-state kinetics of TMR6M-G507C obtained in the present study (Parent et al., 1992b; Eskandari et al., 2005; present study). However, the model failed to describe the presteady-state currents in the absence and presence of sugar and phlorizin, especially their voltage dependence. In particular, the model predicted τ-V relations that are bell shaped (see Fig. 7 B of Hazama et al., 1997), contrary to experimental observations (Fig. 2 C; see also Fig. 4 A of Loo et al., 2005). The eight-state model accounts for the voltage dependence of τ by asymmetric equivalent charge movements ($\varepsilon_{1a} \approx 0$, $\varepsilon_{a1} = 0.5$, $\varepsilon_{ab} = 0.15$, $\varepsilon_{ba} \approx 0$, $\varepsilon_{b6} = 0.05$, $\varepsilon_{6b} = 0.7$). An asymmetric voltage dependence between forward and backward reactions could arise from asymmetric Eyring energy barriers for the transition state (Zagotta et al., 1994). The molecular mechanism for the asymmetry and the location of the voltage sensor(s) in cotransporters such as SGLT1 is unknown. The asymmetry has been observed in the gating currents of shaker Potassium channels (Zagotta et al., 1994; Rodriguez et al., 1998; Schoppa and Sigworth, 1998), but the mechanism is also unknown. One possibility could be a change in the membrane electric field profile between forward and backward reactions (Blunck et al., 2005).

(f) We have previously noted that the model for presteady-state current (Fig. 9, shaded region) failed to account for the kinetics of the fast rising phase ($\tau = 0.17$ ms, Loo et al., 2005), and is due to our assumption of two $Na^+$ ions binding to identical sites with the same rate constant (Falk et al., 1998; Loo et al., 2005). In this study, we found that the model does not correctly predict the fast monotonic decay of presteady-state current and fluorescence for hyperpolarizing pulses from very positive voltages. The simulations predict a biphasic time course in the OFF current when membrane

potential is stepped from a large positive test value to $V_h$ (from +50 to −50 mV). This can be seen in Fig. 11 A, and is a consequence of the high rate ($k_{6b} = 300\ s^{-1}$) and high equivalent charge movement ($\varepsilon_{6b} = 0.7$) from $C_6 \rightarrow C_b$ (see Loo et al., 2005). The discrepancies between model simulations and data are in the submillisecond domain. Resolving the fast kinetic events in $Na^+$ binding remains a major challenge to understanding $Na^+$/glucose cotransport.

(g) The fluorescence changes are primarily associated with the differences in relative quantum yields of the fluorophore in conformations $C_2$, $C_6$, and $C_5$ ($q_{y_5}/q_{y_2} = 3$, $q_{y_6}/q_{y_2} = 6$) because the occupancy probabilities of the other states are low.

### Other Cotransporters

*Charge Movement.* Since our initial observation of presteady-state currents in the $Na^+$/glucose cotransporter (Birnir et al., 1991), they have been observed in many solute carrier (SLC, HUGO Nomenclature) gene families, including SLC1 (high affinity glutamate transporter; Grewer and Rauen, 2005), SLC6 ($Na^+/Cl^-$/GABA; Mager et al., 1993), SLC13 ($Na^+$-sulfate/carboxylate; Chen et al.,1998), SLC15 ($H^+$/oligopeptide; Mackenzie et al., 1996), SLC20 and SLC34 (types II and III $Na^+$/phosphate; Forster et al., 2002), and SLC28 ($Na^+$/nucleoside; Larrayoz et al., 2004, Smith et al., 2004). Common observations are the reduction of presteady-state currents by substrates and the linear relationship between maximal charge ($Q_{max}$) and maximal substrate-coupled current ($I_{max}$), with the ratio ($I_{max}/Q_{max}$) providing an estimate of the turnover rate of cotransporter (for reviews see Forster et al., 2002; Loo et al., 2002; Grewer and Rauen, 2005). We have used charge measurements to probe the conformations of SGLT1 under sugar transport. The positive shift of $V_{0.5}$ with $[sugar]_o$ indicates that the rate-limiting step is $C_5 \rightarrow C_6$. In contrast, we recently found that for hPEPT1 (human $H^+$/dipeptide transporter), glycylsarcosine reduced $Q_{max}$ and shifted $V_{0.5}$ to more negative values (Sala-Rabanal et al., 2006). This negative shift indicates that the rate limiting step is the return of the empty transporter from inward-facing to outward-facing conformation ($C_6 \rightarrow C_1$), unlike the $C_5 \rightarrow C_6$ for hSGLT1. Thus charge measurements in the presence of substrates provide unique and novel insights into the rate-limiting step for cotransporters.

*Voltage Clamp Fluorometry.* Since our initial application of voltage clamp fluorometry to study SGLT1, voltage clamp fluorescence experiments have been performed on the $Na^+/Cl^-$/γ-aminobutyric acid (GAT1; Li et al., 2000; Meinild, A.-K., N. MacAulay, U. Gether, and D. D.F. Loo. 2006. FASEB J. 20:A839), serotonin (SERT; Li and Lester, 2002), glutamate (EAAT3; Larsson et al., 2004), and $Na^+/P_i$ (Virkki et al., 2006) cotransporters. In these studies, with the exception of Li and Lester (2002), the ΔF-V relations are affected by substrates, indicating that substrate interactions alter the distribution of conformations.

### Conclusions

We have used voltage-clamp fluorometry to examine the partial reactions involving sugar binding and transport by the human $Na^+$/glucose cotransporter. This was accomplished using a voltage-jump perturbation protocol in the presence and absence of external sodium, sugar, and phlorizin. Based on simulations of the experimental data using our eight-state, ordered, nonrapid equilibrium, alternating access model (Fig. 9) we conclude that partial reactions involving sugar binding ($k_{23}$, $k_{32}$, $k_{45}$, and $k_{54}$) and $Na^+$/sugar cotransport ($k_{34}$ and $k_{43}$) are neither voltage dependent nor rate limiting. Furthermore, our analysis of presteady-state currents and fluorescence in the presence and absence of sugar or phlorizin demonstrate that: (a) external sugar increases the occupancy probability of inward-facing conformations ($C_5$ and $C_6$) at the expense of outward-facing conformations ($C_2$ and $C_3$); and (b) the high affinity blocker phlorizin locks the cotransporter in an inactive conformation ($C_7$). Finally, under the maximum driving force for inward $Na^+$/glucose cotransport (saturating voltage and external $Na^+$ and sugar concentrations) the rate-limiting step for transport is the electroneutral dissociation of $Na^+$ from the cotransporter at the internal face of the membrane ($C_5$ to $C_6$). In general, our model for cotransport satisfactorily accounts for all the observed steady-state and presteady-state kinetics. The model does not completely account for submillisecond presteady-state kinetics due in part to our assumption that external binding of the two $Na^+$ ions can be simplified by using single lumped rate constants ($k_{12}$ and $k_{21}$). A current challenge is to parse out the rapid kinetics of $Na^+$ binding to the two binding sites.

We thank Mary Lai-Bing, Amanda Johnson, Kari Edwards, Linh Nguyen, and Teresa Ku for the preparation, injection, care of oocytes, and assistance with the uptake experiments. We especially thank Dr. Eric Turk for his help with mutagenesis.

This research was supported by National Institutes of Health grant DK19567.

Olaf S. Andersen served as editor.

Submitted: 3 August 2006
Accepted: 2 November 2006

## REFERENCES

Birnir, B., D.D.F. Loo, and E.M. Wright. 1991. Voltage-clamp studies of the $Na^+$/glucose cotransporter cloned from rabbit small intestine. *Pflugers Arch.* 418:79–85.

Blunck, R., B. Chanda, and F. Bezanilla. 2005. Nano to micro-fluorescence measurements of electric fields in molecules and genetically specified neurons. *J. Membr. Biol.* 208:91–102.

Chen, X.-Z., C. Shayakul, U.V. Berger, W. Tian, and M.A. Hediger. 1998. Characterization of a rat $Na^+$-dicarboxylate cotransporter. *J. Biol. Chem.* 273:20972–20981.

Diez-Sampedro, A., M.P. Lostao, E.M. Wright, and B.A. Hirayama. 2000. Glycoside binding and translocation in $Na^+$-dependent glucose cotransporters: comparison of SGLT1 and SGLT3. *J. Membr. Biol.* 176:111–117.

Diez-Sampedro, A., D.D.F. Loo, E.M. Wright, and B.A. Hirayama. 2004. Coupled sodium-glucose cotransport by SGLT1 requires a negative charge at position 454. *Biochemistry.* 43:13175–13184.

Eskandari, S., E.M. Wright, and D.D.F. Loo. 2005. Kinetics of the reverse mode of the $Na^+$/glucose cotransporter. *J. Membr. Biol.* 204:23–32.

Falk, S., A. Guay, C. Chenu, S.D. Patil, and A. Berteloot. 1998. Reduction of an eight-state mechanism of cotransport to a six-state model using a new computer program. *Biophys. J.* 74:816–830.

Forster, I.C., K. Kohler, J. Biber, and H. Murer. 2002. Forging the link between structure and function of electrogenic cotransporters: the renal type IIa $Na^+/P_i$ cotransporter as a case study. *Prog. Biophys. Mol. Biol.* 80:69–108.

Grewer, C., and T. Rauen. 2005. Electrogenic glutamate transporters in the CNS: molecular mechanism, presteady-state kinetics, and their impact on synaptic signaling. *J. Membr. Biol.* 203:1–20.

Hazama, A., D.D.F. Loo, and E.M. Wright. 1997. Presteady-state currents of the $Na^+$/glucose cotransporter (SGLT1). *J. Membr. Biol.* 155:175–186.

Hirayama, B.A., M.P. Lostao, M. Panayotova-Heiermann, D.D.F. Loo, E. Turk, and E.M. Wright. 1996. Kinetic and specificity differences between the rat, human and rabbit $Na^+$-glucose cotransporters (SGLT-1). *Am. J. Physiol.* 270:G919–G926.

Hirayama, B.A., A. Diez-Sampedro, and E.M. Wright. 2001. Common mechanisms of inhibition for the $Na^+$/glucose (hSGLT1) and $Na^+/Cl^-$/GABA (hGAT1) cotransporters. *Br. J. Pharmacol.* 134:484–495.

Ikeda, T.S., E.-S. Hwang, M.J. Coady, B.A. Hirayama, M.A. Hediger, and E.M. Wright. 1989. Characterization of a $Na^+$/glucose cotransporter cloned from rabbit small intestine. *J. Membr. Biol.* 110:87–95.

Larrayoz, I.M., F.J. Casado, M. Pastor-Anglada, and M.P. Lostao. 2004. Electrophysiological characterization of the human $Na^+$/nucleoside cotransporter 1 (hCNT1) and role of adenosine on hCNT1 function. *J. Biol. Chem.* 279:8999–9007.

Larsson, H.P., A.V. Tzingounis, H.P. Koch, and M.P. Kavanaugh. 2004. Fluorometric measurements of conformational changes in glutamate transporters. *Proc. Natl. Acad. Sci. USA.* 101:3951–3956.

Li, M., and H.A. Lester. 2002. Early fluorescence signals detect transitions at mammalian serotonin transporters. *Biophys. J.* 83:206–218.

Li, M., R.A. Farley, and H.A. Lester. 2000. An intermediate state of the γ-aminobutyric acid transporter GAT1 revealed by simultaneous voltage clamp and fluorescence. *J. Gen. Physiol.* 115:491–508.

Loo, D.D.F., S. Eskandari, K.J. Boorer, H.K. Sarkar, and E.M. Wright. 2000. Role of $Cl^-$ in electrogenic $Na^+$-coupled cotransporters GAT1 and SGLT1. *J. Biol. Chem.* 275:37414–37422.

Loo, D.D.F., A. Hazama, S. Supplisson, E. Turk, and E.M. Wright. 1993. Relaxation kinetics of the $Na^+$/glucose cotransporter. *Proc. Natl. Acad. Sci. USA.* 90:5767–5771.

Loo, D.D.F., B.A. Hirayama, E. Gallardo, J. Lam, E. Turk, and E.M. Wright. 1998. Conformational changes couple $Na^+$ and glucose transport. *Proc. Natl. Acad. Sci. USA.* 95:7789–7794.

Loo, D.D.F., B.A. Hirayama, A.-K. Meinild, G. Chandy, T. Zeuthen, and E.M. Wright. 1999. Passive water and ion transport by cotransporters. *J. Physiol.* 518:195–202.

Loo, D.D.F., S. Eskandari, B.A. Hirayama, and E.M. Wright. 2002. A kinetic model for secondary active transport. *In* Membrane Transport and Renal Physiology. The IMA Volumes in Mathematics and its Applications. Vol. 129. H.E. Layton and A.M. Weinstein, editors. Springer-Verlag, New York. 65–83.

Loo, D.D.F., B.A. Hirayama, A. Cha, F. Bezanilla, and E.M. Wright. 2005. Perturbation analysis of the voltage-sensitive conformational changes of the $Na^+$/glucose cotransporter. *J. Gen. Physiol.* 125:13–36.

Mackenzie, B., D.D.F. Loo, Y. Fei, W.J. Liu, V. Ganapathy, F.H. Leibach, and E.M. Wright. 1996. Mechanisms of the human intestinal $H^+$-coupled oligopeptide transporter hPEPT1. *J. Biol. Chem.* 271:5430–5437.

Mackenzie, B., D.D.F. Loo, and E.M. Wright. 1998. Relationships between $Na^+$/glucose cotransporter (SGLT1) currents and fluxes. *J. Membr. Biol.* 162:101–106.

Mager, S., J. Naeve, M. Quick, C. LaBarca, N. Davidson, and H.A. Lester. 1993. Steady states, charge movements and rates for a cloned GABA transporter expressed in *Xenopus* oocytes. *Neuron.* 10:177–188.

Meinild, A.-K., B.A. Hirayama, E.M. Wright, and D.D.F. Loo. 2002. Fluorescence studies of ligand-induced conformational changes of the $Na^+$/glucose cotransporter. *Biochemistry.* 41:1250–1258.

Panayotova-Heiermann, M., D.D.F. Loo, and E.M. Wright. 1995. Kinetics of steady state and charge movements associated with the rat $Na^+$/glucose cotransporter. *J. Biol. Chem.* 270:27099–27105.

Parent, L., S. Supplisson, D.D.F. Loo, and E.M. Wright. 1992a. Electrogenic properties of the cloned $Na^+$/glucose cotransporter: I. Voltage-clamp studies. *J. Membr. Biol.* 125:49–62.

Parent, L., S. Supplisson, D.D.F. Loo, and E.M. Wright. 1992b. Electrogenic properties of the cloned $Na^+$/glucose cotransporter: II. A transport model under nonrapid equilibrium conditions. *J. Membr. Biol.* 125:63–79.

Quick, M., D.D.F. Loo, and E.M. Wright. 2001. Neutralization of a conserved amino acid residue in the human $Na^+$/glucose transporter (hSGLT1) generates a glucose-gated $H^+$ channel. *J. Biol. Chem.* 276:1728–1734.

Quick, M., J. Tomasevic, and E.M. Wright. 2003. Functional asymmetry of the human $Na^+$/glucose transporter (hSGLT1) in bacterial membrane vesicles. *Biochemistry.* 42:9147–9152.

Rodriguez, B.M., D. Sigg, and F. Bezanilla. 1998. Voltage gating of *Shaker* $K^+$ channels. The effect of temperature on ionic and gating curents. *J. Gen. Physiol.* 112:223–242.

Sala-Rabanal, M., D.D.F. Loo, B.A. Hirayama, E. Turk, and E.M. Wright. 2006. Molecular interactions between dipeptides, drugs and the human intestinal $H^+$-oligopeptide cotransporter hPEPT1. *J. Physiol.* 574:149–166.

Schoppa, N.E., and F.J. Sigworth. 1998. Activation of *Shaker* potassium channels III. An activation gating model for wild-type and V2 mutant channels. *J. Gen. Physiol.* 111:313–342.

Smith, K.M., A.M.L. Ng, S.Y.M. Yao, K.A. Labedz, E.E. Knaus, L.I. Wiebe, C.E. Cass, S.A. Baldwin, X.-Z. Chen, E. Karpinski, and J.D. Young. 2004. Electrophysiological characterization of a recombinant human $Na^+$-coupled nucleoside transporter (hCNT1) produced in *Xenopus* oocytes. *J. Physiol.* 558:807–823.

Toggenburger, G., M. Kessler, and G. Semenza. 1982. Phlorizin as a probe of the small-intestinal $Na^+$, D-glucose cotransporter. A model. *Biochim. Biophys. Acta.* 688:557–571.

Veenstra, M., S. Lanza, B.A. Hirayama, E. Turk, and E.M. Wright. 2004. Local conformational changes in the *Vibrio* $Na^+$/galactose cotransporter. *Biochemistry.* 43:3620–3627.

Virkki, L.V., H. Murer, and I.C. Forster. 2006. Voltage clamp fluorometric measurements on a type II $Na^+$-coupled $P_i$ cotransporter: shedding light on substrate binding order. *J. Gen. Physiol.* 127:539–555.

Zagotta, W.N., T. Hoshi, and R.W. Aldrich. 1994. *Shaker* potassium channel gating III: evaluation of kinetic models for activation. *J. Gen. Physiol.* 103:321–362.

Zampighi, G.A., M. Kreman, K.J. Boorer, D.D.F. Loo, F. Bezanilla, G. Chandy, and E.M. Wright. 1995. A method for determining the unitary functional capacity of cloned channels and transporters in Xenopus laevis oocytes. *J. Membr. Biol.* 148:65–78.